

Chapter 1

Introduction

1.1 Overview of OLED devices and displays

Practical organic light-emitting devices (OLEDs) have been reported by Tang and VanSlyke in 1987. Today, 20 years later, three active-matrix OLEDs (AMOLEDs) were commercialized. In 2004, Kodak-Sanyo demonstrated the first AMOLEDs on the digital camera, as shown in Figure 1-1. They claim OLED is a high-definition image display that is record to none. OLED displays show pictures and video at their best. Bright, clear images and fluid full-motion video appear true-to-life at almost any angle. In 2005, Sony mass produced the first AMOLEDs on the personal digital assistant (PDA) as shown in Figure 1-2. They announced that OLEDs with super top-emission technology is the new thin screens for mobile devices which realize CRT-quality picture clarity and color gamut. Color gamut of 100% and high contrast ratio of 1000:1 were demonstrated. In 2006, BenQ-Siemens announced the first AMOLEDs applied in the mobile phones, S88, as shown in Figure 1-3. Unlike the previous two products which are meteoric in the market, the quantity of S88 is large. The responses from the market are also encouraging. The feedbacks from the user we

heard are: *The S88's OLED display is quite remarkable; you have to see it to believe it.*

Even though it is only 176 x 220, it is incredibly bright and extremely color-saturated.

It is absolutely gorgeous.



Figure 1-1 The first full color AMOLED product of DSC demonstrated by Kodak-Sanyo in 2004.



Figure 1-2 The first AMOLED product of PDA demonstrated by Sony in 2005.



Figure 1-3 The first full color AMOLED product of mobile phone demonstrated by BenQ-Siemens (AUO) in 2006.

1.2 Motivation

OLEDs are considered to be the best display technology in the world. Compared with the common LCD display, OLED display intrinsically has wide viewing angle, high contrast ratio, and is brighter, self-emitting and thin. To further maximize the advantages of the OLED display, it is necessary to develop the top-emitting OLEDs (TOLEDs). Compared with bottom-emitting OLEDs, TOLEDs have higher efficiency and color gamut due to the microcavity effect in the devices. Because light emits from the surface of substrate, the aperture ratio (AR) of the pixels will not be sacrificed by the wire and TFT circuits as shown in Figure 1-4. For a set luminance, larger AR allows the pixel driven at a lower current leading to much higher operational lifetime of the displays. In addition, introducing white-light TOLEDs (WTOLEDs) can eliminate the precision shadow mask and AR can be even larger than 60%.

There is another key advantage for the TOLED display at the power consumption of OLED display can be as low as half of that of LCDs. Power consumption of the panel will be the key issue for portable devices because the multimedia application will be integrated in a mobile phone. Long-time watching TV, playing music video with mp3, 3G communications and DSC displaying in a single device result in high power utilization of the panel. The advantage of OLED displays is that power consumption of the panel is only dependent on the pixels that are lit in

the images displayed. This is excellent for power consumption of the display.

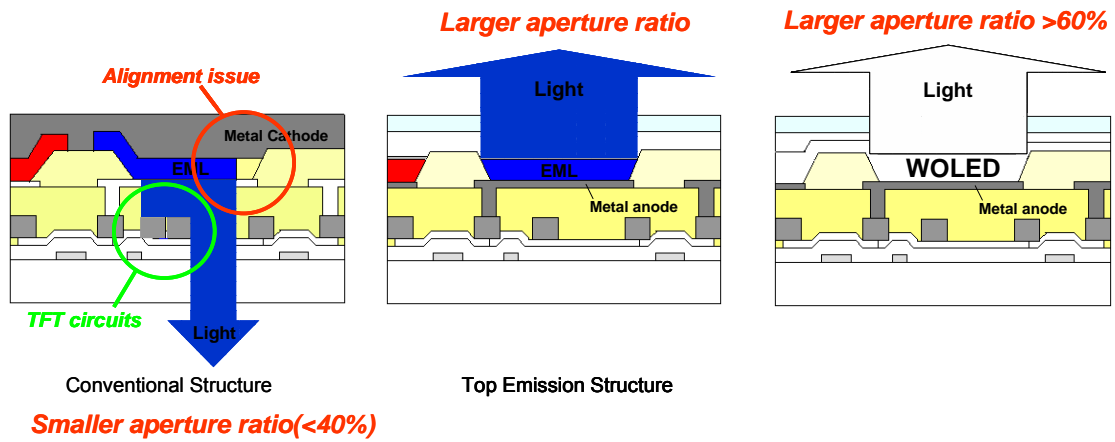


Figure 1-4 Comparison of bottom-emitting and top-emitting devices.











					
OLED	52 mW	174 mW	62 mW	36 mW	40 mW
LCD	200 mW	200 mW	200 mW	200 mW	200 mW
					
OLED	31 mW	45 mW	64 mW	23 mW	284 mW
LCD	200 mW	200 mW	200 mW	200 mW	200 mW

Figure 1-5 Dynamic power consumption of AMOLEDs.

As shown in Figure 1-5, the power of all images are almost lower than 60 mW, while the LCD with backlights consume essentially constant power of 200 mW disregarding the images that are displayed. By calculation, the average power

consumption for displaying dynamic images is only about 30% of that of LCDs. An optical enhancement in a TOLED can improve the efficiency. Two times efficiency enhancement compared with bottom-emitting device is always obtained in TOLEDs. Therefore, in terms of power, 50% power-saving can be easily achieved in TOLEDs.

1.3 Thesis outlines

In this thesis, we introduce several top-emitting OLEDs including RGB and white-light emission. All TOLEDs were optimized by electrode modification and interference adjustment of the devices to achieve high efficiency.

In chapter 2, we optimized the microcavity effect in RGB TOLEDs by adjusting the thickness of ITO. Preliminary results show potentially TOLEDs with higher efficiency and color saturation.

In chapter 3, we further optimized reflectivity of electrodes, thickness of organic layers, and hole-injection property of the devices and achieve highly efficient RGB TOLEDs.

In chapter 4, we fabricated the WTOLEDs with a modified anode, and a highly transparent cathode. By alleviating the undesirable microcavity effect in the device, we can obtain the highly efficient WTOLEDs with very broad emission.

In chapter 5, we demonstrated the WTOLEDs using a single blue dopant,

DSA-Ph, with the residual emission from Alq. By tuning the optical length of the devices, we can demonstrate an easy way to fabricate WTOLEDs.

Finally, we summarized in chapter 6 and discuss the future prospects for OLEDs.



Chapter 2

Color-saturated top-emitting organic light-emitting devices

2.1 Introduction

For full color active matrix organic light-emitting devices (OLEDs), a backplane thin-film transistors (TFT) design that provides a constant and uniform drive current is very important. The uniformity issue can be resolved by incorporating four or more TFTs in combination with one capacitor in the drive circuit [1-2]. But, the increase in the number of TFTs fabricated on the substrate will invariably reduce the aperture ratio (AR) of each pixel of a bottom-emitting OLED that would in turn require a much higher drive current density in order to achieve the same level of luminance for display with pixels of larger AR.

Top-emitting organic electroluminescent devices (TOLEDs), unlike conventional ones, are structurally not effected by the number of TFTs integrated on the substrate as light will emit from the top as all electrical circuits and TFTs can be hidden below the reflective ITO/Ag anode. As a result, the AR of TOLEDs can be greatly increased

and the operating voltage reduced for a given luminance that could ultimately result in longer operational lifetime of the device.

Furthermore, in order to meet the requirements of a properly balanced white emission of a full color display, the color purity and saturation of each red, green and blue (RGB) subpixel are also critical. In a recent report of projected performance targets for the basic diode needs in high-resolution OLED displays of the future [3], it was suggested that the Commission Internationale de L'Eclairage chromaticity coordinates ($CIE_{x,y}$) of red, green and blue devices are $x > 0.7$, $y > 0.75$ and $(x+y) < 0.22$, respectively. The reason is that with increasing saturation of each subpixel of primary RGB emissions, the total power consumption for white light for a given luminance can be reduced [4]. Unfortunately, these target goals are not easy to achieve for most known organic luminescent materials because they tend to have broad EL peak with large full width at half maxima (FWHM) about 70-100 nm, which often leads to reduction of color saturation. In the literature, microcavity effect has been explored to modify the color emissions of OLED [5-13]. According to the model, Sony Corp. has developed a Top-emission Adaptive Current drive (TAC) scheme, which was reported to improve the color saturation of the red OLED [14-15]. In this paper, color-saturated and highly efficient TOLEDs were developed with reflective double-layer silver (Ag)/indium-tin oxide (ITO) as anode because of the high

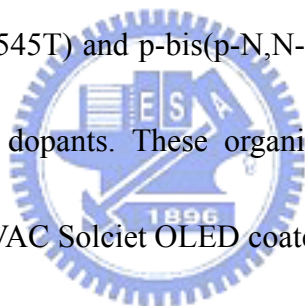
reflectance of silver and the desired work function of ITO. Double-layer Ca/ Ag were adopted as damage-free cathode which is deposited by thermal evaporation to eliminate sputtering-induced radiation damages. In addition, optical length of microcavity can be tuned by adjusting the thickness of organic layer and our ITO anode. To the best of our knowledge, no report has been documented on adjusting the emissions of all three primary RGB colors to near National Television Systems Committee (NTSC) saturation by microcavity effect on TOLEDs using simple ITO thickness optimization and the judicious choice of fluorescent dopants.

2.2 Experimental



In our experiments, the general structure of our TOLEDs is shown in Figure 2-1 where ITO thin film is deposited by low-power radio-frequency Magnetron sputtering. The sputtering power is fixed at 300 W and the chamber is full with Ar atmosphere at 0.5 Pa. Thicknesses of ITO were determined by the sputtering time. Before device fabrication, the indium-tin-oxide (ITO)-coated glasses were followed the routine cleaning procedure of ultrasonicing in organic solvents, deionized water, and dried in oven at 120 °C, the ITO substrate was then loaded on the grounded electrode of a parallel-plate plasma reactor, pretreated by oxygen plasma, and then selectively coated with a polymerized fluorocarbon film. In addition, copper phthalocyanine

(CuPc) and 4,4'-bis[N-(1-naphthyl)-N-phenyl-amino]biphenyl (NPB) were adopted as the hole injection layer and hole transporter layer, respectively. Aluminum tris(8-hydroxyquinoline) (Alq) was adopted both as the electron transport material and the host emitter for red and green dopants while 2-(*t*-butyl) di-(2-naphthyl)anthracene (TBADN) [16] was used as the host for blue dopants. 2-{2-(*t*-butyl)-6-[(E)-2-(1,1,7,7-tetramethyl-2,3,6,7-tetrahydro-1H,5H-pyrido [3,2,1-*ij*]quinoline-9-yl)-1-ethenyl]-4H-4-pyranliden}malonitrile (DCJTb), 10-(1,3-benzothiazol-2-yl)-1,1,7,7-tetramethyl-2,3,6,7-tetrahydro-1H,5H,11H-pyrano[2,3-*f*]pyrido [3,2,1-*ij*]quinoline-11-one (C-545T) and *p*-bis(*p*-N,N-di-phenyl-aminostyryl) benzene (DSA-Ph) are used as RGB dopants. These organic materials were deposited by thermal evaporation in an ULVAC Solciet OLED coater at a base vacuum of 10^{-7} Torr. Ca and Ag thin films were fabricated similarly in the separate chamber. All devices were hermetically sealed prior to testing. The active area of the EL device, defined by the overlap of the ITO and the cathode electrodes, was 9 mm^2 . The reflectance spectra were recorded on a Steag ETA-Optik spectrometer; electroluminescent (EL) spectra, luminance yield and $\text{CIE}_{x,y}$ color coordinates were measured by a Photo Research PR-650 spectrophotometer driven by a programmable dc source.



2.3 Results and discussions

2.3.1 Alq-based devices with various thickness of ITO

Different thicknesses of ITO varying from 50, 75, 100, 125 and 150 nm were sputtered onto Ag (100 nm) to find the optimized reflective anode property and their reflectance spectra were measured, accordingly. All of the five thin-film samples showed similar response throughout the visible range (400-900 nm) with high reflectance (~80%). However, upon fabricating TOLEDs using these anodes with sequential deposition of CuPc, NPB, Alq and semitransparent cathode layers with fixed thickness, dramatic differences in EL spectra and device performance were observed as depicted in Figure 2-2. When ITO was 50 nm, the EL of Alq peaks at 500 nm and its FWHM was narrowed to only 36 nm. When ITO was increased to 75 nm, the EL peak shifts 516 nm without changing the FWHM. The red-shift was continued when ITO increased to 100 nm, 125 nm and 150 nm with the EL peaks appeared near 572 nm, 608 nm and 664 nm respectively. The EL spectra of device with 150 nm of ITO peaks are 664 nm with a very broad shoulder near 570 nm and an additional small peak at 470 nm. These results can be rationalized by the cavity effect of the ITO layer as by tuning the thickness of ITO, the EL spectra is shifted in a wide range (from 500 to 664 nm) and the shape of the EL spectra is also changed.

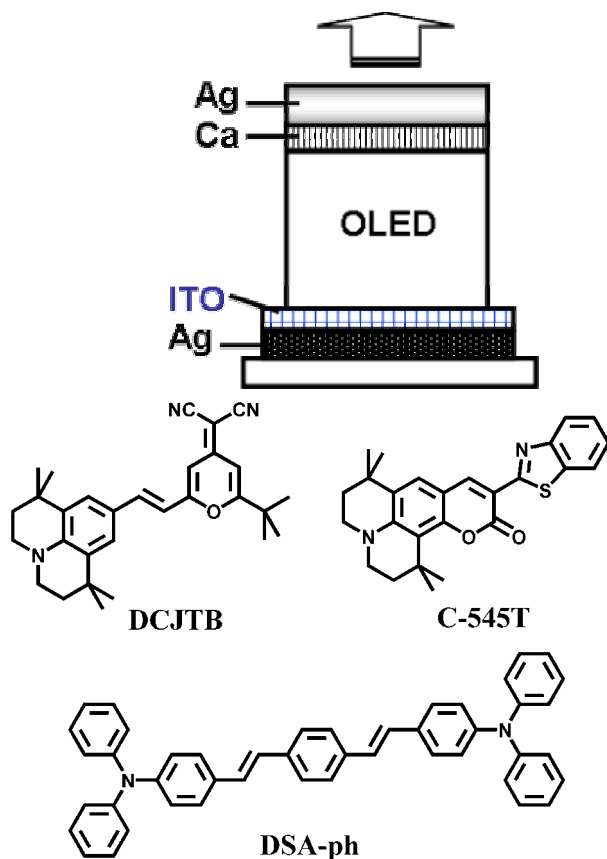


Figure 2-1 The device structure of the TOLED and molecular structures of the three dopants (DCJTB, C-545T and DSA-Ph).

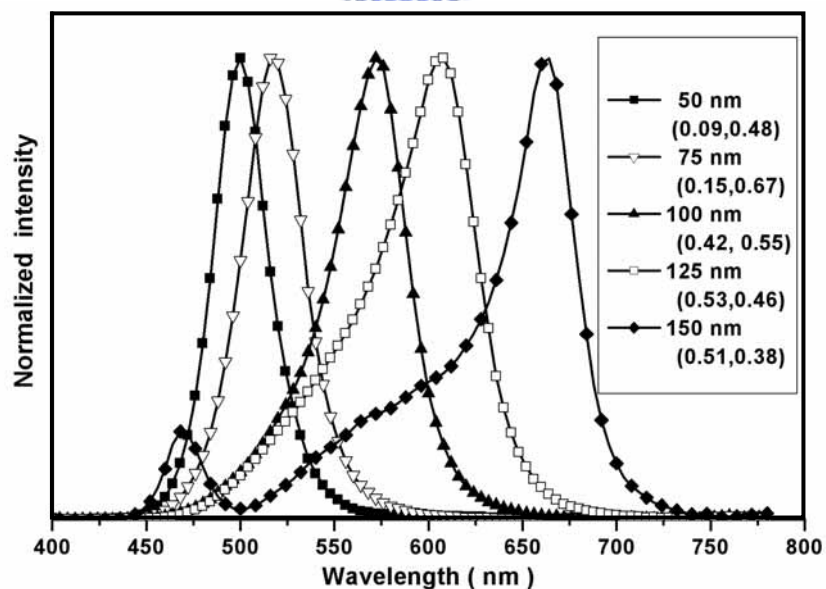


Figure 2-2 Normalized EL spectra and 1931 CIE_{x,y} coordinates of TOLEDs with four different thickness of ITO in the ITO/Ag anode.

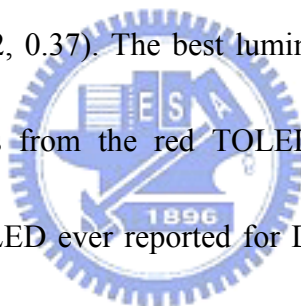
The corresponding color change of this Alq-based TOLED emitter in term of $CIE_{x,y}$ is shown in the insert of Figure 2-2. Using the simple interference law: $n_{int}L + L_{penetration} = \lambda/2$, we expect that EL spectra of these TOLEDs changes with: $n_{ITO}\Delta L_{ITO} = \Delta \lambda/2$. It matches our experimental results.

2.3.2 Optimized TOLEDs with RGB emissive colors

To exploit the microcavity effect of this device, several well-known fluorescent dopants are doped into the TOLEDs. Thus, DCJTB, C-545T, and DSA-Ph are used as red, green and blue dopants, respectively, whose molecular structures and PL spectra are showed in Figures 2-1 and 2-3, respectively. The RGB structure of our TOLEDs are Ag (100 nm)/ ITO (x nm)/ CF_x/ NPB (120 nm)/ 40% Alq : 60% rubrene : 2% DCJTB (30 nm)/ Alq (50 nm)/ Ca (5 nm)/ Ag (15 nm), Ag (100 nm)/ ITO (x nm)/ CuPc (15 nm)/ NPB (60 nm)/ Alq : 1% C-545T (37.5 nm)/ Alq (37.5 nm)/ Ca (5 nm)/ Ag (15 nm), Ag (100 nm)/ ITO (x nm)/ CuPc (15 nm)/ NPB (40 nm)/ TBADN+ 5% DSA-Ph (20 nm)/ Alq (20 nm)/ Ca (5 nm)/ Ag (15 nm), respectively. All of the organic and cathode layers are constant when ITO thickness varies. By changing the thickness of ITO, the optimized thickness of ITO was chosen to be 75 nm in all of the doped devices. The performances of these devices are listed in Table I and their EL spectra are plotted in Figure 2-4.

Contrary to the bottom-emitting devices, we found the TOLEDs doped with 2%

DCJTB, 1% C-545T, and 5% DSA-Ph show sharper RGB emissions at 608, 514, and 464 nm with FWHM of only 28, 28, and 32 nm, respectively. As can be observed, the emissive colors of all of the doped TOLEDs are purer and more saturated than those of the bottom-emitting ones. The green C-545T doped TOLED shows a luminance efficiency of 9.2 cd/A and saturated color of CIE_{x,y} (0.14, 0.75). In blue device, highly saturated color is also achieved with CIE_{x,y} (0.14, 0.08), but the efficiency (0.9 cd/A) is not as good as one would like. Although higher efficiency (3.0 cd/A) of blue device can be fabricated with increased thickness of ITO (100 nm), the color is shifted to bluish green with CIE_{x,y} (0.12, 0.37). The best luminance yield (7 cd/A) and power efficiency (4.8 lm/W) comes from the red TOLED, which is the most efficient fluorescent dye-doped red OLED ever reported for DCJTB. Comparing at the same doping concentration and color saturation of CIE_{x,y} (0.64, 0.36), the best result from the bottom-emitting DCJTB doped co-host emitter was 4.5 cd/A [19].



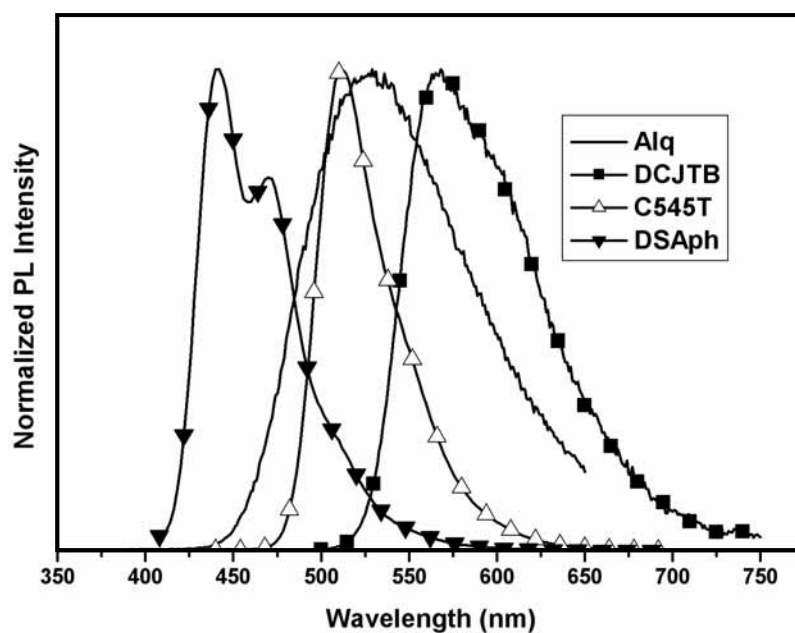


Figure 2-3 PL spectra of Alq, DCJTb, C545T and DSA-Ph.



Table I. EL performance of DSA-Ph, C-545T, and DCJTb doped top-emitting OLEDs (The three devices with 75 nm of ITO are measured at 20 mA/cm², while the other device is measured at 133 mA/cm². The RGB dopants are DSA-Ph, C-545T, and DCJTb for blue, green, and red devices, respectively.).

Thickness of ITO	Dopant	Voltage (V)	Efficiency (cd/A)	1931 CIE		FWHM (nm)
				x	y	
100 nm	Blue	10.0	3.0	0.12	0.37	52
75 nm	Blue	7.1	0.9	0.14	0.08	28
75 nm	Green	10.0	9.2	0.14	0.75	28
75 nm	Red	6.51	7.0	0.64	0.36	32

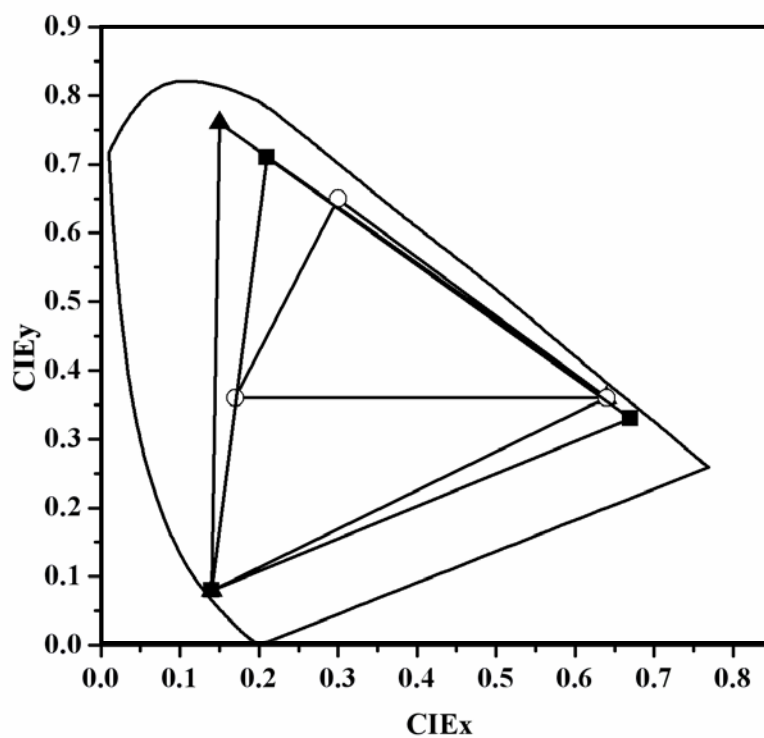
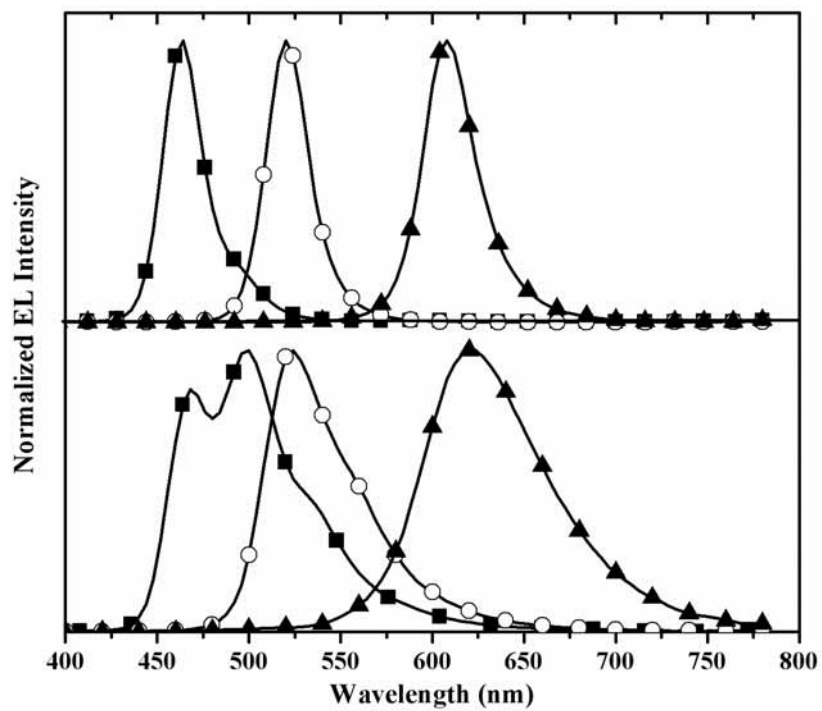
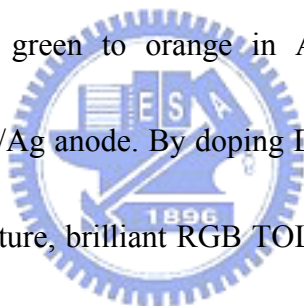


Figure 2-4 (a) Normalized EL spectra of top-emitting (upper) and bottom-emitting (lower) OLEDs doped with DCJTB (▲), C-545T (○) and DSA-Ph (■). (b) The color gamut achieved by TOLED (▲) and bottom-emitting OLED (○) are compared with that of NTSC (■).

2.3.3 Viewing angle of Alq-based and RGB TOLEDs

In this section, viewing angles of Alq-based and RGB TOLEDs consisting of 75nm of ITO are measured. Luminances vs. viewing angle curves are plotted in Figure 2-5. Because of strong microcavity effect, luminance of all TOLEDs reduces to less than half of initial intensity when viewing angle is larger than 45°. Therefore, although microcavity effect enhances luminance yields and color saturation of these TOLEDs, the effect also limits their viewing angles.

In summary, we demonstrated color-saturated and highly efficient TOLEDs with different colors from bluish green to orange in Alq-based device by changing thicknesses of ITO in the ITO/Ag anode. By doping DCJTb, C-545T and DSA-Ph in the microcavity adjusted structure, brilliant RGB TOLEDs can be obtained with pure and saturated colors that are comparable to NTSC standard.



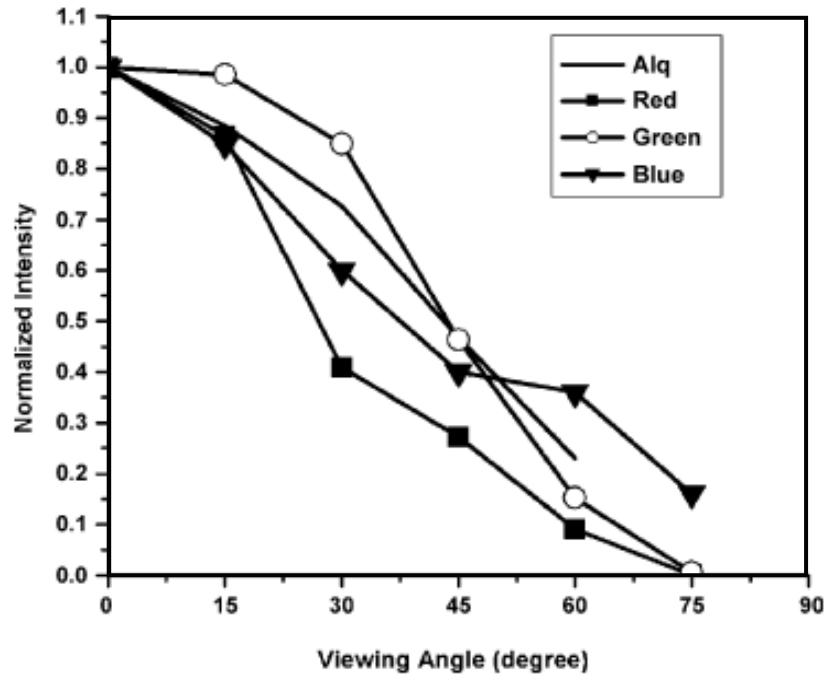


Figure 2-5 Viewing-angle properties of Alq-based and RGB TOLEDs consisting of 75 nm of ITO as the anode.



References

- [1] J. H. Lee, W. J. Nam, S. M. Han, M. K. Han, *SID Digest*, **34** (2003) 490.
- [2] J. C. Goh, C. K. Kim, J. Jang, *SID Digest*, **34** (2003) 494.
- [3] J. N. Bardsley, United States Display Consortium, San Jose, CA 95113, 2002.
[http://www.usdc.org/technical/downloads/OLED_Techroadmap_nbtext.pdf]
- [4] H. K. Chung, *IDW Digest*, **9** (2002) 12.
- [5] A. Dodabalapur, L. J. Rothberg, T. M. Miller, E. W. Kwock, *Appl. Phys. Lett.* **64** (1994) 2486.
- [6] A. Dodabalapur, L. J. Rothberg, T. M. Miller, *Electron. Lett.* **30** (1994) 1000.
- [7] A. Dodabalapur, L. J. Rothberg, T. M. Miller, *Appl. Phys. Lett.* **65** (1994) 2308.
- [8] N. Takada, T. Tsutsui, S. Saito, *Appl. Phys. Lett.* **63** (1993) 2032.
- [9] S. Tokito, K. Noda, Y. Taga, *Appl. Phys. Lett.* **68** (1996) 2633.
- [10] P. E. Burrows, V. Khalfin, G. Gu, S. R. Forrest, *Appl. Phys. Lett.* **73** (1998) 435.
- [11] R. B. Fletcher, D. G. Lidzey, D. D. C. Bradley, M. Bernius, S. Walker, *Appl. Phys. Lett.* **77** (2000) 1262.
- [12] F. Jean, J. Y. Mulot, B. Geffroy, C. Denis, P. Cambon, *Appl. Phys. Lett.* **81** (2002) 1717.
- [13] A. Dodabalapur, L. J. Rothberg, R. H. Jordan, T. M. Miller, R. E. Slusher, J. M. Phillips, *J. Appl. Phys.* **80** (1996) 6954.

- [14] T. Sasaoka, M. Sekiya, A. Yamoto, J. Yamada, T. Hirona, Y. Iwase, T. Yamada, T. Ishibashi, T. Mori, M. Asano, S. Tamura, T. Urabe, *SID Digest*, **32** (2001) 384.
- [15] S. Terada, G. Izumi, Y. Sato, M. Takahashi, M. Teda, K. Kawase, K. Shimotoku, H. Tamashiro, N. Ozawa, T. Shibasaki, C. Sato, T. Nakadaira, Y. Iwase, T. Sasaoka, T. Urabe, *SID Digest*, **34** (2003) 1463.
- [16] B. Balaganesan, W. J. Shen, C. H. Chen, *Tetrahedron Lett.* **44** (2003) 5747.
- [17] C. Y. Iou, T. H. Liu, H. H. Chen, W. J. Shen, C. H. Chen, *SID Digest*, **34** (2003) 971.
- [18] C. H. Chen, C. W. Tang, *Appl. Phys. Lett.* **79** (2001) 3711.
- [19] T. H. Liu, C. Y. Iou, C. H. Chen, *Appl. Phys. Lett.* **83** (2003) 5241.



Chapter 3

Highly efficient top-emitting organic light-emitting devices

TOLEDs have the advantage of improving color saturation and luminance efficiency because of strong microcavity effect produced between the two electrodes.

A device with NTSC color gamut over 100% was often observed in TOLEDs.

Furthermore, the enhancement of device efficiency in the normal direction reduces power consumption of the display effectively. As a result, highly efficient RGB

TOLEDs are one of the most promising technologies to meet the requirements of mobile display applications.



3.1 Optical simulation

The principal of microcavity is realized that the spontaneous emission resonates in a cavity composed of the total reflective mirror and semitransparent thin film, only certain wavelength is allowed cavity modes, and emits light in a given direction.

Intensity enhancement and spectral narrowing are the most common phenomena

caused by microcavity effect. Taking the advantage of microcavity effect, high efficiency devices with saturated color can be achieved easily.

Figure 3-1 shows calculated luminance intensity of RGB microcavity devices as a function of NPB hole-transport-layer thickness by the Fabry-perot rule. As higher carrier mobility of HTL than that of ETL, tuning NPB thickness in a reasonable range won't sacrifice device voltage. The modeled structure is glass/Ag (100 nm)/NPB (vary) /EML (30 nm)/Alq (30 nm)/Ag (20 nm). The curves show the luminance predicted by theoretical model for blue (460 nm), green (530 nm), and red (640 nm) emitting layers. Thin hole-injecting or electron-injecting layers were neglected which are irrelevant from an optical point of view. The simulated results show the RGB devices with intense intensity when NPB thickness are 85, 55 and 45 nm, respectively.

It is noted that intensity of the red device is stronger than those of green and blue one.

This implicates that light of shorter wavelength tends to be trapped in the device.

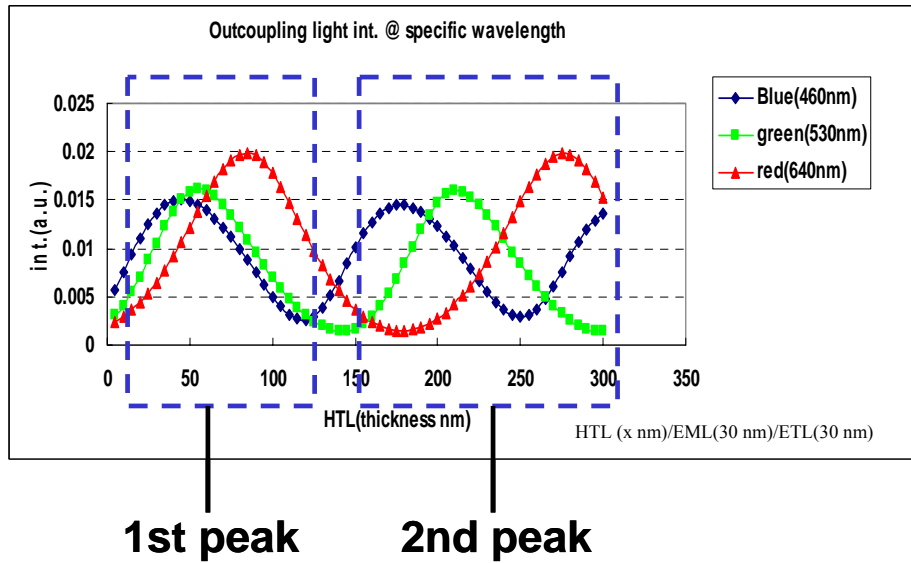


Figure 3-1 Calculated luminance intensity of RGB microcavity devices as a function of NPB hole-transport-layer thickness.

3.2 High efficiency TOLED devices

The device structures of three top-emitting devices were designed and fabricated as shown in Figure 3-2. In Device **A** of the conventional top-emitting device, 200-nm-thick Ag as reflective anode coated with a polymerized fluorocarbon film (CF_x) as hole-injection layer was used and Ca/Ag was used as semi-transparent cathode. A device of structure NPB (vary) /EML (30 nm)/Alq (30 nm) for organic layers are fixed. Compared with Device **A**, Ca was replaced by an n-doped ETL in Device **B**. Finally, in Device **C**, two new hole-injection materials, HIM1 and HIM2 were used to place of CF_x . Optical length of all devices were optimized for RGB with proper thickness of NPB.

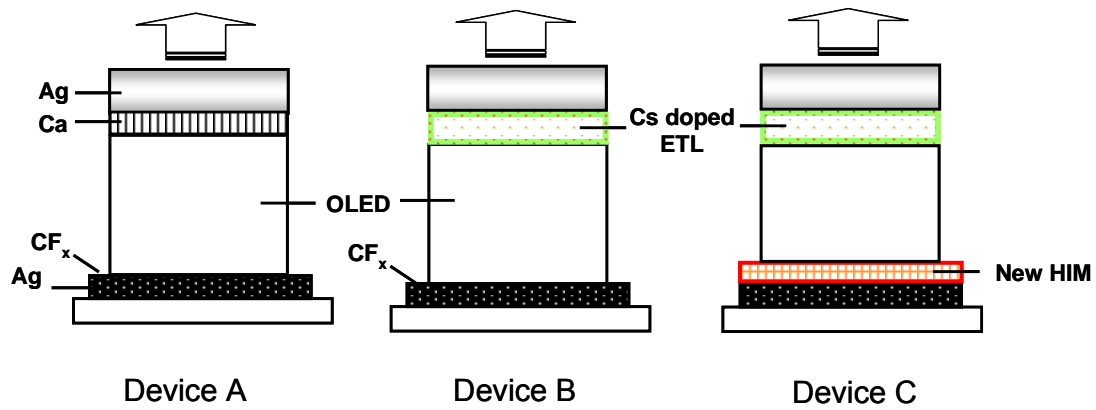


Figure 3-2 Device architecture of the three top-emitting devices. A (Ca/Ag system), B (n-doping ETL/Ag system) and C (New-HIMs).

3.2.1 Ca/Ag system

Device **A** is our first-type device structure for TOLEDs in which DCJTB, C545T and DSA-Ph are the dopants for RGB emissive layers. The RGB devices were optimized with fixed EML and ETL and different thickness of NPB according to simulation results. RGB devices show the best efficiency as NPB thicknesses are 60, 50 and 10 nm, respectively. Table I shows detailed EL performance of RGB devices. DCJTB doped in co-host consisting of Alq and rubrene, a luminance yield of 17.4 cd/A with $CIE_{x,y}$ coordinates of (0.67, 0.33) has been achieved. Green and blue devices with luminance yields of 26.7 and 3.7 cd/A and the corresponding $CIE_{x,y}$ of (0.22, 0.72) and (0.12, 0.18) were demonstrated, respectively. Compared with color gamut of 65% in a bottom-emitting device, high color gamut of 92% was observed.

Table I. EL performance of RGB devices measured at 20 mA/cm² (Device A).

	Dopants	Color	Efficiency
Top	DCJTB	R (0.67, 0.33)	17.4 cd/A
	C545T	G (0.22, 0.72)	26.7 cd/A
	DSAPh	B (0.12, 0.18)	3.7 cd/A

3.2.2 N-doping ETL/Ag system

In mass production consideration, evaporation of Ca metal is not compatible with existing manufacturing process. An n-doped ETL combined with metal cathode were employed instead in the second type TOLEDs, as Device **B** in which we replaced Ca/Ag to Cs-doped ETL/Ag cathode. A phosphorescent red dopant, ER33, a deep blue dopant, EB512 and a deep blue host EB46 were introduced in the TOLEDs. All these materials are commercially available by e-ray optoelectronics and detailed chemical structures were also under the protection of e-ray optoelectronics' proprietary. The detailed EL performances of top and bottom-emitting RGB devices are compared in Table II and CIE colors and EL spectra of RGB TOLEDs are plotted in Figures 3-3 and 3-4. Highly saturated color of CIE_{x,y} (0.646, 0.353), (0.227, 0.721) and (0.135, 0.056) for RGB, respectively were demonstrated and shown a NTSC color gamut of 102%. High efficiencies of the green and red TOLEDs of 26.2 and 31.5 cd/A which are more than 2 times higher than those of the bottom-emitting devices were achieved. Blue devices with CIE_{x,y} color of (0.132, 0.139) and (0.135, 0.056) reaching

luminance yields of 3.8 cd/A and 1.5 cd/A, respectively were also achieved. Although the blue devices show relatively lower luminance efficiency than that of the bottom-emitting device, stronger radiance of much deeper blue devices with CIE_y exceeding NTSC blue color was demonstrated for the first time.

Table II. Comparison of EL performance between bottom and top emitting devices measured at 20 mA/cm² (Device B).

	Color	Efficiency
Top	R (0.646, 0.353)	31.5 cd/A
	G (0.227, 0.721)	26.2 cd/A
	B (0.132, 0.139)	3.8 cd/A
	B (0.135, 0.056)	1.5 cd/A
Bottom	ER33 R (0.647, 0.349)	11.5 cd/A
	C545T G (0.320, 0.640)	12 cd/A
	EB512-G B (0.144, 0.163)	5 cd/A

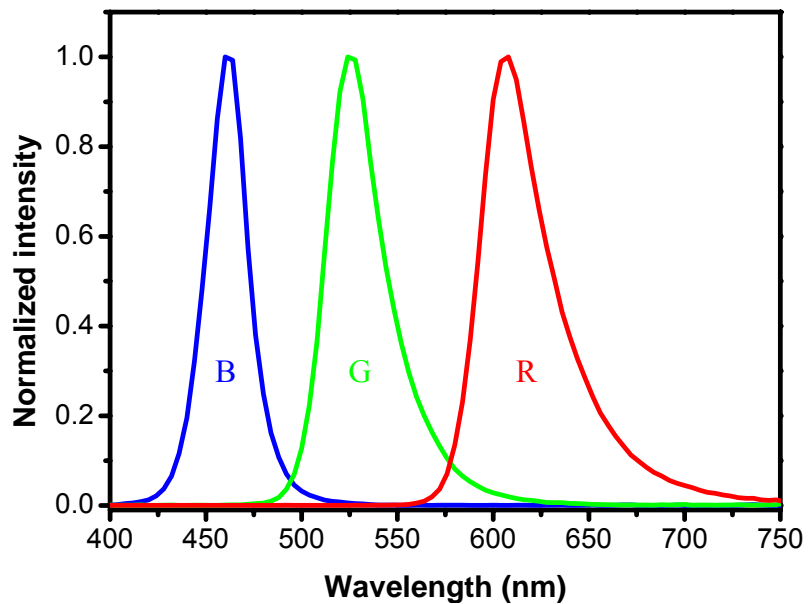


Figure 3-3 Narrow EL spectra of RGB emission from type 2 device structure.

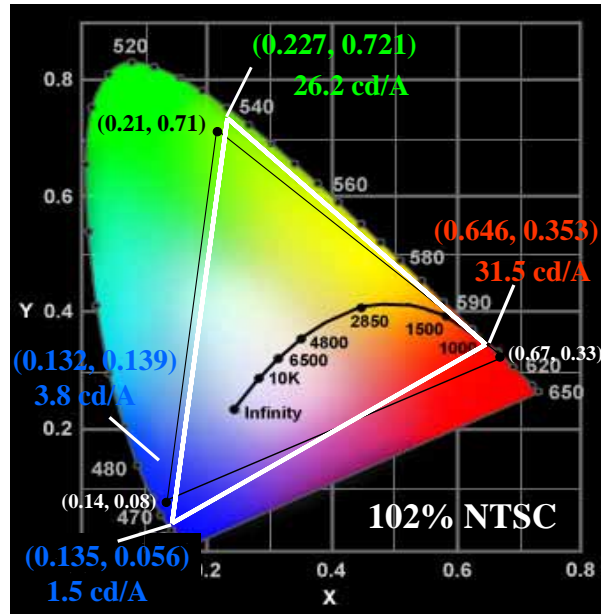


Figure 3-4 Saturated CIE colors of RGB devices (Device B).



Table III shows detailed EL performance of RGB devices using device structures B. It is also particularly noted that optimal thickness of NPB for RGB devices are 60, 40 and 160 nm, respectively. Introducing n-doping ETL system does change position of emission dipole of the device. That is the reason why there is slightly different in thickness of NPB between Devices **A** and **B**. A thick NPB thickness of 160 nm was the second mode of optimal optical length for blue emission. Using thick NPB layer is also good advantage for avoiding the dark point issue in an active-matrix platform.

3.2.3 New HIMs system

Contrary to the Device **B**, we replaced CF_x and introduced two new hole-injection materials, HIM-1 and HIM-2, to develop the third type TOLEDs whose structure is shown as Device **C**. $Ag:NPB/WO_3$ is the HIM1 and $WO_3:NPB/WO_3$ is the HIM2. Figure 3-5 shows the energy diagrams of these HIMs. Ag doped NPB layer provides quite good work function alignment property and WO_3 doped NPB layer increase the hole concentration. We found these new HIMs not only improve hole-injection from metal anode, Ag, but also provide good hole and electron balances in the TOLEDs. Efficiencies of RGB device were shown in Table IV. The same RGB dopants were used as in Device **B**. We demonstrated that we can achieve similar chromaticity (NTSC 105%) but the better luminance efficiency than that of Device **B**. In particular, the efficiency of the red device using HIM-1 and HIM-2 reached 37.5 cd/A and 39.3 cd/A, respectively. We believe that these red TOLEDs' luminance efficiencies with more than 3 times enhancement were among the best ever reported in the literatures. Not only efficiency and color saturation are improved, but also driving voltage. Table V shows driving voltage for the green device at a luminance of 1000 nits with three different HIMs. Using HIM-1 and HIM-2 as hole injection layer, a significantly improvement of driving voltage around 1.5-2 V was achieved.

Compared with the Ag anode, Al or AlNd are widely used in TFT backplane.

Highly reflective Al or AlNd were also good candidates as the anode for TOLEDs. However, low work function of 3.8 eV of Al and AlNd leads to high energy barrier between the anode and hole-transporting layer, resulting in high driving voltage. This issue is urgent to be circumvented to meet the requirement of AMOLEDs application. Our two new HIMs can also solve the problem. Figure 3-6 shows the *J-V* characteristics comparisons of different hole-injection layers on the Al anode. The device structure is Al/HIL/NPB (60 nm) /Alq (65 nm) /2% Cs₂CO₃:Alq (10 nm)/Ag (20 nm). The thickness for HIM1 and HIM2 are 5 nm, and 2% F4-TCNQ doped layer as the HIL is 15 nm. Devices using HIM1 and HIM2 have driving voltage reduction of 5 V, compared with common F4-TCNQ doped HIL. Moreover, 10 V reduction in voltage between new HIMs and pure Al anode is significantly improved. As a result, the efficient hole-injection property of these two HIMs provides a good opportunity to facilitate AMOLEDs with the TOLED technology.

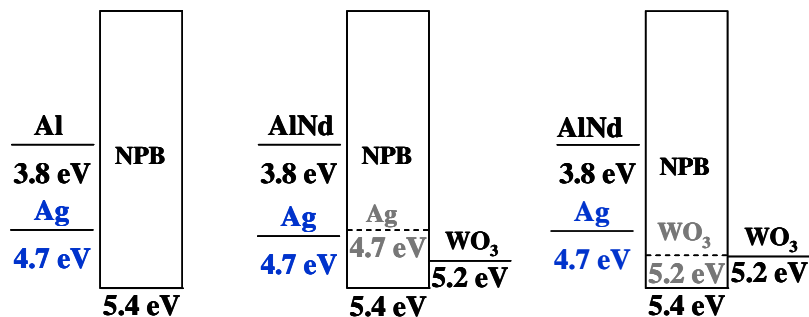


Figure 3-5 Energy diagrams of HIM1 and HIM2.

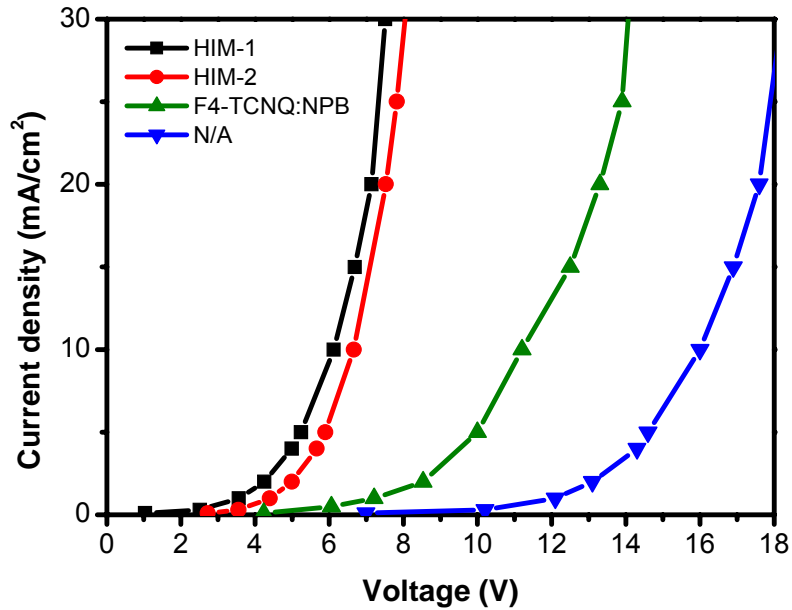
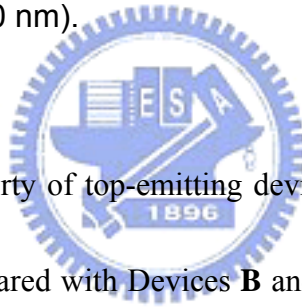


Figure 3-6 *J-V* characteristics comparisons of different hole-injection layer on the Al anode. The device structure is Al/HIL/NPB (60 nm) /Alq (65 nm) /Cs₂CO₃:Alq (10 nm)/Ag (20 nm).



The viewing angle property of top-emitting devices is always highly concerned for a full color display. Compared with Devices **B** and **C** in Tables III and V, there is also a large improvement from 10% to 30%. This can be rationalized that our new HIMs with different optical properties from organic layer results in better light coupling. Although light-outcoupling of 30% at viewing angle of 60 degree is still not satisfied, color change is encouraged. A CIE color shift of 0.05 is the maximum tolerance for human eyes. All devices show a good CIE color shift smaller than 0.05. Red and Blue devices are even better. A CIE shift of 0.02 for red and 0.03 for blue were achieved. Figure 3-7 shows the EL spectra of green device under different viewing angle. This is the evidence shows there is no significant color change under

different viewing angles. The intensities of RGB colors show similar decay at viewing angle from 0 to 60 degree. This also implicates that there is *no* viewing angle problem in top-emitting devices. As RGB TOLEDs have very high contrast and maintain good colors, images still can be displayed clearly.

Table III. Detailed EL performance of RGB devices (Device B).

Devices	Voltage (V) @ 1000 nits	Wavelength (nm)	FWHM (nm)	Yield(%) at 60°	Δ CIE(x,y) at 60°
R NPB600	4.4	600	44	13%	± 0.02 (0.630, 0.368)
G NPB400	6.3	528	36	11%	± 0.05 (0.193, 0.670)
B NPB1600	7.5	468	24	6%	± 0.03 (0.160, 0.030)

Table IV. EL performance of RGB using new HIMs measured at 20 mA/cm².

	Color	Efficiency
HIM-1	R (0.640, 0.359)	37.5 cd/A
	G (0.229, 0.722)	24.7 cd/A
	B (0.125, 0.082)	2.1 cd/A
HIM-2	R (0.623, 0.376)	39.3 cd/A
	G (0.210, 0.730)	32.1 cd/A
	B (0.141, 0.045)	1.8 cd/A

Table V. Comparison of three hole-injection materials in green devices.

Devices	Voltage (V) @ 1000 nits	Yield(%) at 60°	Δ CIE(x,y) at 60°
HIM-1	4.8	31%	0.05
HIM-2	4.1	28%	0.05
CF _x	6.3	11%	0.05

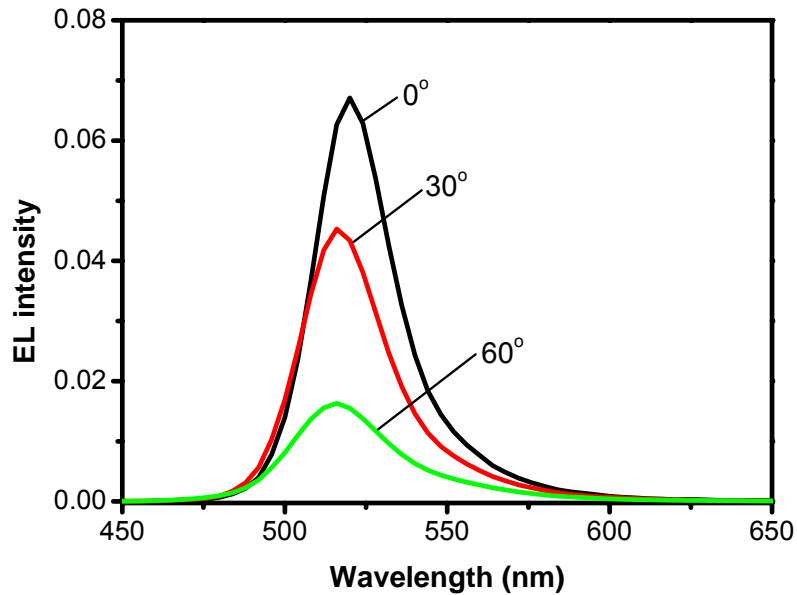


Figure 3-7 EL spectra of green device (device C-HIM2) under viewing angle of 0°, 30° and 60° off the surface normal.

3.3 Power consumption simulation of TOLEDs

The power consumptions and white-light efficiency of these TOLEDs with different device structure were simulated. We calculated panel power with assumption of 2" display with 176 x 220 pixels, brightness of 150 nits, white CIE coordinates (0.31, 0.32) and Vd-s is 12V. The transmittance of the polarizer is 44%. To mix a white light, the first thing needs to be confirmed is that the ratio of GRB emission intensity. Assume the three colors of RGB with CIE coordinates are (x_r, y_r) , (x_g, y_g) and (x_b, y_b) , respectively. As the definition of CIE1931, color coordinates can be represented as follows:

$$\left\{ \begin{array}{l} x_r = \frac{X_R}{X_R + Y_R + Z_R} \\ y_r = \frac{Y_R}{X_R + Y_R + Z_R} \\ z_r = \frac{Z_R}{X_R + Y_R + Z_R} = 1 - x_r - y_r \end{array} \right. \quad \left\{ \begin{array}{l} x_g = \frac{X_G}{X_G + Y_G + Z_G} \\ y_g = \frac{Y_G}{X_G + Y_G + Z_G} \\ z_g = \frac{Z_G}{X_G + Y_G + Z_G} = 1 - x_g - y_g \end{array} \right.$$

$$\left\{ \begin{array}{l} x_b = \frac{X_B}{X_B + Y_B + Z_B} \\ y_b = \frac{Y_B}{X_B + Y_B + Z_B} \\ z_b = \frac{Z_B}{X_B + Y_B + Z_B} = 1 - x_b - y_b \end{array} \right.$$

$$\text{set } S_R = X_R + Y_R + Z_R \quad S_G = X_G + Y_G + Z_G \quad S_B = X_B + Y_B + Z_B$$

A color can be mixed with different ratios of RGB and represented as



$$\begin{bmatrix} X \\ Y \\ Z \end{bmatrix} = \begin{bmatrix} X_R & X_G & X_B \\ Y_R & Y_G & Y_B \\ Z_R & Z_G & Z_B \end{bmatrix} \begin{bmatrix} R \\ G \\ B \end{bmatrix}$$

The equation can be also written as

$$\begin{bmatrix} X \\ Y \\ Z \end{bmatrix} = \begin{bmatrix} x_r S_R & x_g S_G & x_b S_B \\ y_r S_R & y_g S_G & y_b S_B \\ z_r S_R & z_g S_G & z_b S_B \end{bmatrix} \begin{bmatrix} R \\ G \\ B \end{bmatrix}$$

RGB colors mix a white light

$$\begin{bmatrix} X_w \\ Y_w \\ Z_w \end{bmatrix} = \begin{bmatrix} x_r S_R & x_g S_G & x_b S_B \\ y_r S_R & y_g S_G & y_b S_B \\ z_r S_R & z_g S_G & z_b S_B \end{bmatrix} \begin{bmatrix} R \\ G \\ B \end{bmatrix}$$

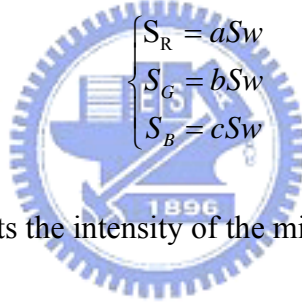
Assume the CIE color of the white light is (0.31, 0.32), then

$$\left\{ \begin{array}{l} x_w = \frac{X_w}{X_w + Y_w + Z_w} = 0.31 \\ y_w = \frac{Y_w}{X_w + Y_w + Z_w} = 0.32 \\ z_w = \frac{Z_w}{X_w + Y_w + Z_w} = 1 - 0.31 - 0.32 = 0.37 \end{array} \right.$$

Set $S_w = X_w + Y_w + Z_w$, thus

$$\left\{ \begin{array}{l} 0.31S_w = x_r S_R + x_g S_G + x_b S_B \\ 0.32S_w = y_r S_R + y_g S_G + y_b S_B \\ 0.37S_w = z_r S_R + z_g S_G + z_b S_B \end{array} \right.$$

and the solutions of S_R , S_G and S_B can be written as function of S_w , that is,



$$\left\{ \begin{array}{l} S_R = aS_w \\ S_G = bS_w \\ S_B = cS_w \end{array} \right.$$

By definition, Y represents the intensity of the mixed color

$$Y = y_r S_R \cdot R + y_g S_G \cdot G + y_b S_B \cdot B = a y_r S_w \cdot R + b y_g S_w \cdot G + c y_b S_w \cdot B$$

Then, to mix a white light, the ratio of RGB intensity is $a y_r : b y_g : c y_b$. As we

know the brightness of the panel, we can calculate the actual intensities of RGB

emission, respectively. The transmittance of the polarizer should be also considered.

The currents for RGB pixels can be calculated with RGB current efficiencies

separately. Assume the voltage for TFT and OLED is 12 V, and total current for the

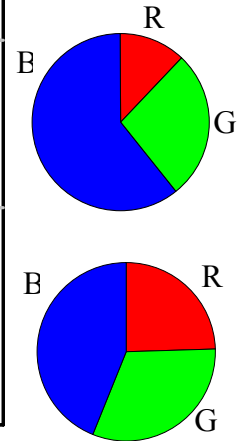
panel is calculated as previous, the power consumption can also be available.

The detailed results are listed in Tables VI and VII. In Device **B**, the white-light efficiency and power were significantly improved from 8.7 cd/A and 188 mW in the bottom-emitting device to 11.8 cd/A and 139 mW. We also concerned the effect in the device performance of two different colors of blue in Device **B**. Although device with deeper blue emission has lower current efficiency, devices show similar performances in the white-light efficiency and the power consumption. It is also the evidence shown that the radiance of low-efficiency deep blue color is still sufficient to form efficient white-light emission.

Table VII shows the simulation results of the Device **C**. A very high efficiency of 16.3 cd/A and low power consumption of 101 mW were delivered in the device using HIM2. The powers of different devices were plotted in Figure 3-8. Compared with commercial 2" LCD, a 50% power-saving target was achieved. 45% power reduction compared with bottom-emitting OLEDs was also accomplished. We believe that OLEDs with lower power consumption can be further improved by introducing higher efficiency emitters, such as phosphorescent green emitters.

Table VI. Efficiency and power simulation of Device B.

	Color	Efficiency	White efficiency	Power (30%loading)
Top	R (0.646, 0.353)	31.5 cd/A	11.8 cd/A	139 mW
	G (0.227, 0.721)	26.2 cd/A		
	B (0.132, 0.139)	3.8 cd/A		
	B (0.135, 0.056)	1.5 cd/A		
Bottom	ER33 R (0.647, 0.349)	11.5 cd/A	8.7 cd/A	188 mW
	C545T G (0.320, 0.640)	12 cd/A		
	EB512 B (0.144, 0.163)	5 cd/A		



Assumptions

- 2" display, 150nits white (0.31, 0.32)
- Vd-s 12 V



Table VII. Efficiency and power simulation of Device C.

	Color	Efficiency	White efficiency	Power (30%loading)
HIM-1	R (0.640, 0.359)	37.5 cd/A	11.6 cd/A	142 mW
	G (0.229, 0.722)	24.7 cd/A		
	B (0.125, 0.082)	2.1 cd/A		
HIM-2	R (0.623, 0.376)	39.3 cd/A	16.3 cd/A	101 mW
	G (0.210, 0.730)	32.1 cd/A		
	B (0.141, 0.045)	1.8 cd/A		

Assumptions

- 2" display, 150nits white (0.31, 0.32)
- Vd-s 12 V

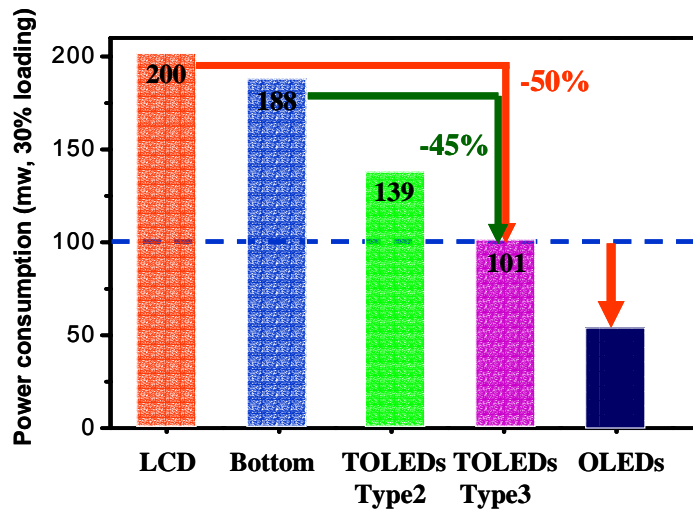


Figure 3-8 Power consumption comparisons of different devices.

3.4 WTOLEDs on TFT array

The top-emitting OLED structure was integrated with a 2” QCIF+ (176 x 222) LTPS-TFT substrate and fabricated by AU optoelectronics. Figure 3-9 shows the photo images of the panel. It is to be noted that panel shows highly saturated colors in RGB and images are vivid with very high contrast.

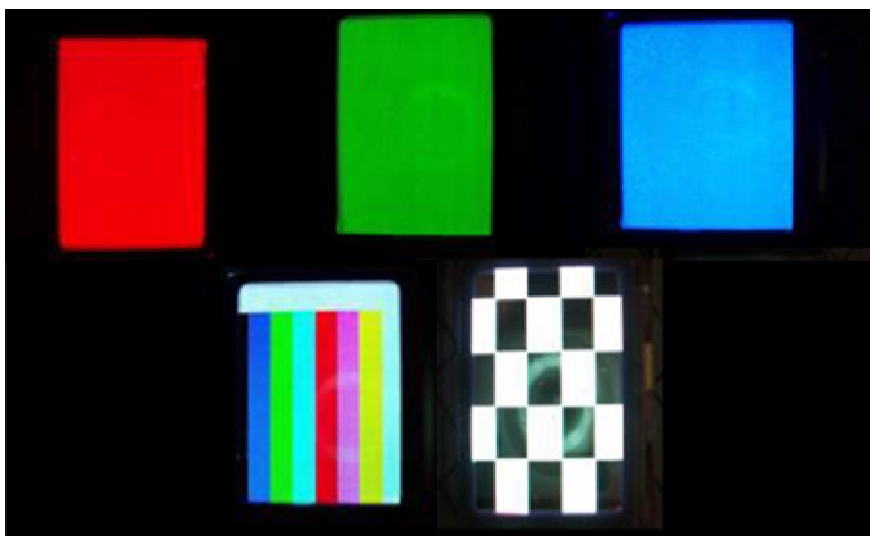


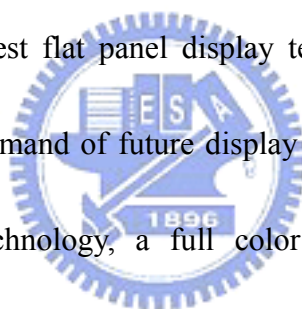
Figure 3-9 Photo of TOLEDs on LTPS-TFT backplane.

Chapter 4

White light top-emitting organic light-emitting devices

4.1 Introduction

Organic light-emitting devices (OLEDs) (Ref. 1) have been well recognized in recent years as one of the best flat panel display technologies that are capable of meeting the most stringent demand of future display applications. To realize the full potential of this display technology, a full color top-emitting OLED structure (TOLED) coupled with a low temperature poly-silicon (LTPS) thin film transistor (TFT) active matrix backplane appears to be the most attractive. This is because TOLED can provide not only higher aperture ratio (AR) than the usual bottom emitting one, but also higher display image quality that often necessitates a more complicated drive circuit in active matrix OLEDs (AMOLEDs). In addition, it is also well established that pixels with high AR in the panel invariably lead to prolonged operational stability owing to less current density needed to drive each pixel in order to achieve a desired luminescence. In recent years, there also has been considerable



interest in developing high-efficiency white OLEDs. This is because it provides the full color AMOLEDs with the alternative approach using white OLEDs coupled with color filter (CF) that can circumvent the problematic shadow mask for red-green-blue (RGB) pixelation in production and achieve a much higher display resolution. This led Sanyo/Kodak to declare in 2003 that white-light OLEDs with a on-chip CF and LTPS-TFT combined with top emission architecture will be the most attractive full color OLED technology in the future [2]. However, it remains a challenge to generate white-light over a *broad* range of the visible spectrum in top-emitting OLEDs because it is unavoidably interfered with by a strong microcavity effect. To the best of our knowledge, no report has been documented on generating highly efficient *broadband* white-light emissions in a top-emitting device.



In SID 2004, Sony demonstrated a full color display with vivid images employing a “super top emission” scheme which was combined with a white emitter, microcavity structure, and CF array [3], in which a three-wavelength white-light was adjusted under a specific optical length to optimize the microcavity effects in the respective RGB pixels. Although a white emitter was used, individual RGB light, instead of *broad* white emission, was created by patterning three different thicknesses of indium-tin oxide (ITO). In mass production consideration, the requirements of a three-wavelength white light coupled with three different and matching thicknesses of

ITO patterned on one substrate could be difficult and not compatible with an existing manufacturing process.

A microcavity structure in a top-emitting device is formed between a reflective anode and a semitransparent cathode, and the microcavity effect can be realized as one kind of Fabry-Perot filter which should satisfy the following equation:

$$\frac{2L}{\lambda_{\max}} + \frac{\Phi}{2\pi} = m \quad (m = \text{integer}), \quad (1)$$

where L is the optical length between the two mirrors, and Φ is the sum of the phase shift from anode and cathode [4].

The full width at half maximum (FWHM) (Refs. 5 and 6) can be estimated by

$$FWHM = \frac{\lambda^2}{2L} \times \frac{1 - \sqrt{R_1 R_2}}{\pi(R_1 R_2)^{1/4}}, \quad (2)$$

where R_1 and R_2 are the reflectance of the two mirrors. Spectral narrowing is the most common phenomena caused by a strong microcavity effect. As implied from Eq. (2), a shorter L as well as lower R_1 or R_2 are preferred to alleviate the undesirable microcavity effect and to obtain wider FWHM emission. In order to study the optical interference in the white-light top-emitting device, we fabricated the devices with a modified anode, and a highly transparent cathode.

4.2 White light top-emitting organic light-emitting devices with a dual-cavity structure

In our previous study, the microcavity phenomena of TOLEDs were observed when we adopted Ca/Ag as semitransparent cathode and Al/ITO as reflective anode. By taking advantage of this microcavity effect in TOLEDs, devices which emit all three primary colors could be fabricated respectively. Since microcavity structure always reduces the full width at half maxima (FWHM), it becomes disadvantageous to fabricate a white light TOLED which often requires a broad emission for display applications. To alleviate this problem, we explore and report herewith a novel dual-cavity structure which consists of a partition layer inserted between the organic layers and reflective anode to attenuate the white light composition.

In our experiments, the three different structures of OLEDs studied are shown in Figure 4-1 where ITO thin film is deposited by low-power RF sputtering, copper phthalocyanine (CuPc) was thermally evaporated as the hole injection layer while 4,4'-bis[*N*-(1-naphthyl)-*N*-phenyl-amino]biphenyl (NPB) was the hole transport layer as well as the host emitter for the yellow dopant. Aluminum *tris*(8-hydroxyquinoline) (Alq) was adopted as the electron transport material and 2-(*t*-butyl)-*di*(2-naphthyl)anthracene (TBADN) [7] was used as the host for blue dopant. Yellow and blue dopants were rubrene and *p*-bis(*p*-*N,N*-di-phenyl-amino)styryl)benzene

(DSA-Ph), respectively. These organic materials were deposited by thermal evaporation in an ULVAC Solciet OLED coater at a base vacuum of 10^{-7} Torr. Al, Ca and Ag thin films were fabricated similarly in the separate chamber. Electroluminescent (EL) spectra, luminance yield and 1931 Commission Internationale de L'Eclairage chromaticity coordinates ($CIE_{x,y}$) were measured by a Photo Research PR-650 spectrophotometer.

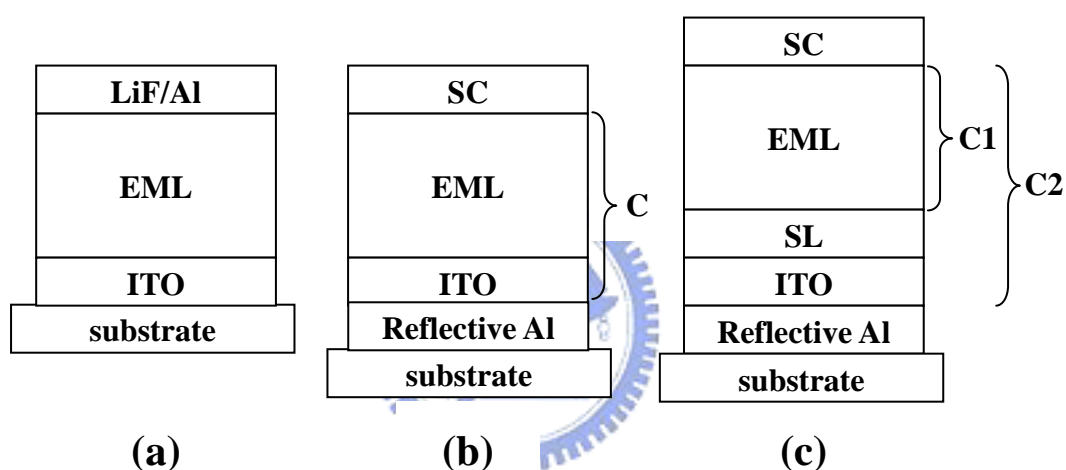


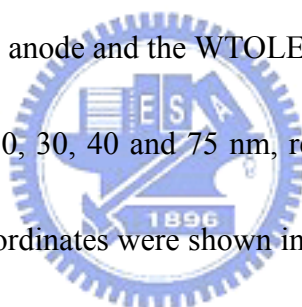
Figure 4-1 Concept of (a) bottom-emitting, (b) single-cavity top-emitting and (c) dual-cavity top-emitting OLEDs. SC, EML and SL represent semi-transparent cathode, emitting layer and separating layer, respectively. C, C1 and C2 represent cavities.

4.2.1 Single-cavity WTOLEDs

In bottom-emitting OLEDs, high-efficiency white light has been demonstrated by Kodak [8]. Our two-element white light was fabricated by doping the yellow rubrene followed by a blue light-emitting layer which is made of TBADN doped with

DSA-Ph. The anode was made of Al, ITO and Ni, and 5 nm Ca and 15 nm Ag were fabricated as semitransparent cathode. While, ideal white light is difficult to achieve for most known organic luminescent materials in TOLED due to the poor color purity of blue light which tends to have broad EL peak with large full width at half-maxima (FWHM), brilliant individual R, G, B color can be readily obtained in the microcavity-adjusted structure. Thus, taking the advantage of TOLEDs, we can tune a microcavity structure to emit deep blue and mix with the proper ratio of yellow light to achieve ideal white light.

First, Al/ITO was used as anode and the WTOLEDs were fabricated with Al with varying thickness of ITO of 10, 30, 40 and 75 nm, respectively. The EL spectra and corresponding $CIE_{x,y}$ color coordinates were shown in Figure 4-2. The intensity of two main colors were found to increase and decrease with different thickness of ITO. With increasing thickness of ITO, $CIE_{x,y}$ coordinates of the emission shifted from yellow to blue which passed through the white light region. When thickness of ITO reached 10 nm, the emissive color of the TOLED was like that of the yellow dopant, rubrene.



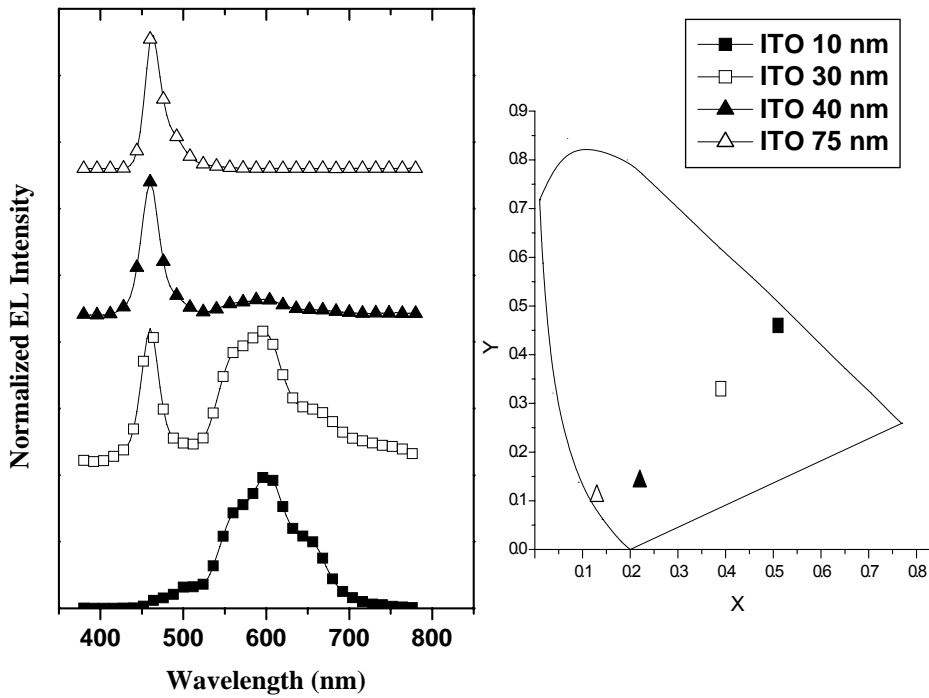


Figure 4-2 The EL spectra and 1931 CIE_{x,y} diagram of white TOLED using Al/ITO as anode. The thickness of ITO is 10, 30, 40 and 75 nm, respectively.

Comparatively, when ITO was 75 nm, the emissive color of the TOLED was like that of the blue dopant, DSA-Ph with CIE_{x,y} coordinates of (0.51, 0.45) and (0.13, 0.11), respectively. The blue-emissive TOLED showed a narrow EL peak at 464 nm due to a relatively strong microcavity effect. Furthermore, when ITO thickness was 30 nm, its CIE_{x,y} coordinate was (0.39, 0.33) which was close to the coordinate of white light (0.33, 0.33). But, when thickness of ITO increased slightly to 40 nm, the CIE color was shifted to (0.22, 0.14) which became too blue for white. The experimental results therefore prove that color of WTOLEDs is very sensitive to the thickness variation of ITO and ideal white light production with CIE_{x,y} (0.33, 0.33) is by no

means easy in a top-emitting architecture.

To study the effect of reflective anode, we also fabricated TOLEDs with Ni and Al as the anodes. Ni with a high work function of 5.4 eV is of particular interest as anodes with high work function can improve the hole-injection ability and device performances [9]. Because work function of Ni is as high as 5.4 eV, so devices using Ni as the anode were also studied. In our experiments, Ni was coated onto Al layer by thermal deposition. Different anodes of devices were fabricated with Al and Ni whose thickness varies from 10 nm, 45 nm and 75 nm, respectively. EL spectra and CIE_{x,y} values were shown in Figure 4-3. All of these three devices showed most by yellow with little blue light. The 1931 CIE_{x,y} coordinates were all around (0.48, 0.48). This result can be attributed to low reflectivity of nickel, especially in the blue spectral region [18]. White light is also not easy to obtain in this device because significant disparity between the reflectivity of the yellow and blue colors. However, it is noticed that higher luminance was indeed obtained in Al/Ni (10 nm) device than the other two devices. The reason is that most light passed through the nickel thin film and is reflected by the highly reflective aluminum. In Al/Ni (75 nm) device, most light is reflected by thick nickel itself so the luminance is not as good as that of Al/Ni (10 nm). Poor light transmittance and reflectivity cause low luminance in Al/Ni (45 nm) device.

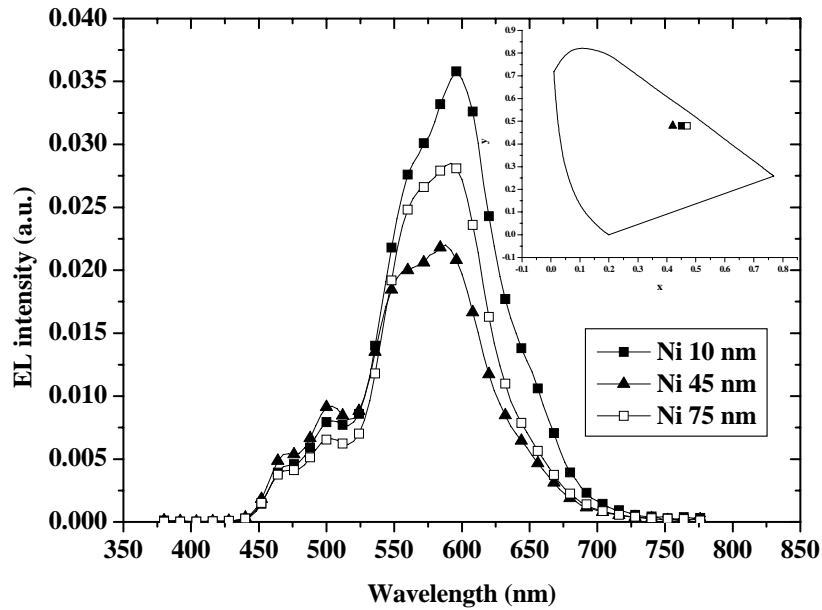


Figure 4-3 The EL spectra and 1931 CIE_{x,y} diagram of white TOLED using Al/Ni as anode. The thickness of Ni is 10, 40 and 75 nm, respectively.



4.2.2 Simulation and experimental comparisons of single-cavity WTOLEDs

The principal of microcavity can be realized by the spontaneous emission that resonates in a cavity composed of the total reflective mirror and semi-transparent thin film, from which only certain wavelength is allowed in cavity modes, and emits light in a given direction. Intensity enhancement and spectra narrowing are the most common phenomena caused by microcavity effect.

In our devices, the reflective mirror is contributed by the 100-nm-thick Al with more than 80% reflectivity throughout the visible region. Semitransparent cathode is the combination of two layers of calcium and silver with proper thickness. Optical length of the cavity is given by [6,11]

$$L = \frac{\lambda}{2} \left(\frac{n}{\Delta n} \right) + \sum_i n_i L_i + \left| \frac{\phi_m}{4\pi} \lambda \right|, \quad (3)$$

where λ is the free-space wavelength, n_i and L_i are the refractive index and thickness of each layer between the electrodes, respectively, n and Δn are the effective refractive index and the index difference between Ca and Ag, and ϕ_m is the phase change at reflective Al. The contribution of optical length is more obvious in different thickness of ITO because of larger refractive index ($n=2.2$) than that of organic layer ($n=1.6 \sim 1.7$). By changing the optical length of the device, we can tune the emissive color systematically.

The EL spectrum of TOLED, $E_c(\lambda)$, can be easily simulated using the following equation:

$$|E_c(\lambda)|^2 = \frac{(1-R_d) \sum_i \left[1 + R_m + 2(R_m)^{0.5} \cos\left(\frac{4\pi x_i}{\lambda}\right) \right]}{1 + R_m R_d - 2(R_m R_d)^{0.5} \cos\left(\frac{4\pi L}{\lambda}\right)} |E_n(\lambda)|^2, \quad (4)$$

where R_1 and R_2 are the reflectivities of cathode and anode, respectively, x_i is the effective distance of the emitting layer from reflective Al, and $E_n(\lambda)$ is an EL spectrum of bottom-emitting OLEDs with the same structure of organic layers. In our case, due to two emitting elements, we have x_1 and x_2 which are represented to blue light emissive region and yellow light emissive region, respectively.

In Figure 4-4, our simulation result is compared with bottom-emitting and top-emitting OLEDs. It is found that the simulation result is very similar to the EL

spectrum of TOLED which has a maximum emission peak around 470 nm and only a slight shoulder appeared around 500 and 560 nm. Therefore, it appears the microcavity model of our TOLEDs can be readily simulated with good matching result.

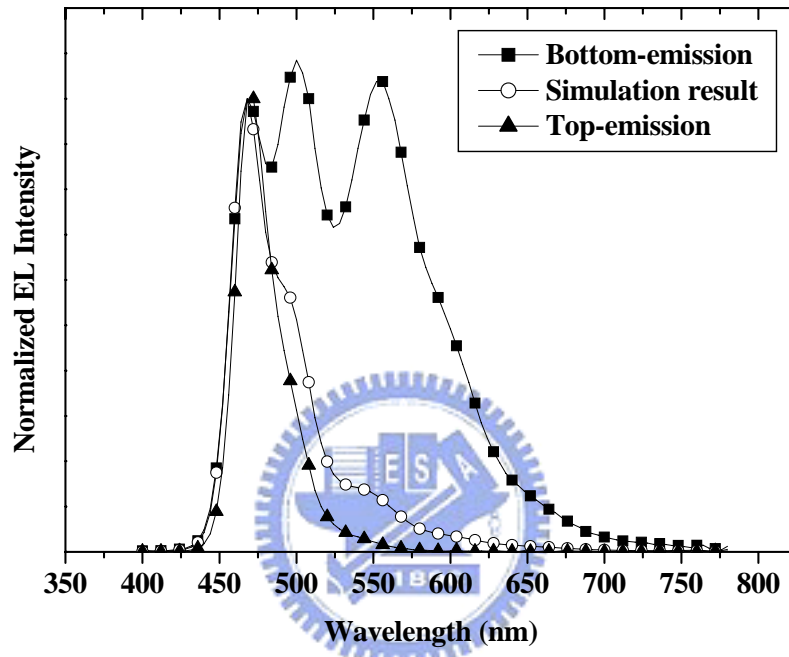


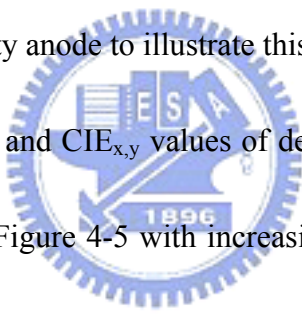
Figure 4-4 The EL simulation and experimental comparison of OLEDs with the same structure of organic layers.

4.2.3 Using Al/ITO as the separating layer in a dual-cavity structure

Since two-emitter TOLEDs with Al/ITO or Al/Ni as the anode are not easily tuned to produce white light because only specific wavelength of light could be enhanced in a single microcavity structure, we introduce herewith a novel dual microcavity structure by different combination of the anode which allows two colors additively to generate white light. The EL emission characteristics of two distinctive

emissive lights were investigated by the multilayer of Al/ITO/Al/ITO and Al/ITO/Ni as the anode, respectively.

The dual-cavity anode is composed of two sets of Al and ITO. The bottom-side cavity is optimized for blue light and the top-side cavity is suitable for yellow light. Thickness of separating Al within these two cavities is controlled to allow the quantity of blue light to penetrate and yellow light to reflect. By properly adjusting the respective thickness of Al/ITO, the ratio of blue and yellow lights can be tuned systematically. Thus, the combination of Al (100 nm)/ITO (50 nm) and Al/ITO (10 nm) is chosen as the dual-cavity anode to illustrate this effect.



The EL spectra character and $CIE_{x,y}$ values of device with different thickness of separating Al were shown in Figure 4-5 with increasing of Al thickness, intensity of blue emission decreases and yellow emission increases slowly. Thicker Al reflects more yellow light and allows less blue light to transmit which shifts the $CIE_{x,y}$ color coordinate from (0.13, 0.11) to (0.30, 0.46). The detail of EL performance is shown in Table I. The data suggests that the ratio of blue and yellow emission can be tuned, but it still can not produce a white light. We believe that a white TOLED can be obtained, however, with proper thickness of ITO and using the same methodology to adjust the length of the cavity between Al.

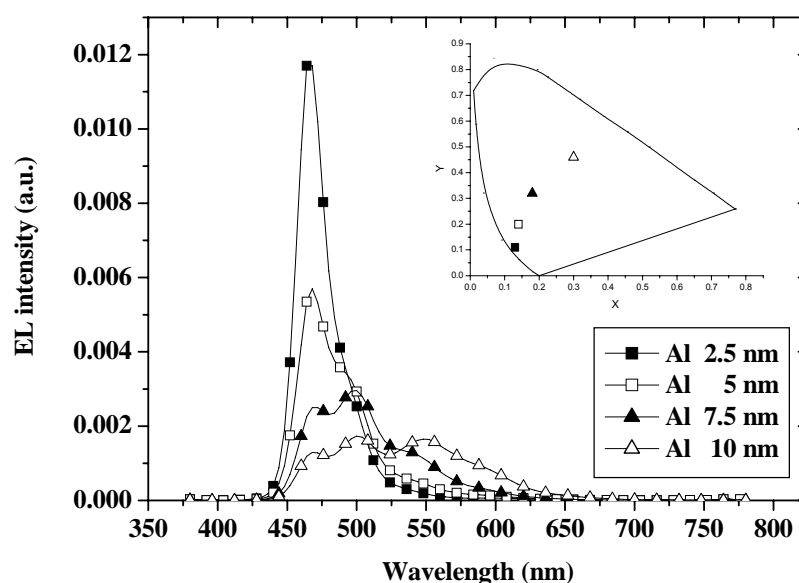


Figure 4-5 The EL spectra and 1931 CIE_{x,y} diagram of dual-cavity white TOLED using Al (100 nm)/ITO (50 nm) and Al/ITO (10 nm) as anode and separating layer, respectively. The thickness of Al of the separating layer is 2.5, 5, 7.5 and 10 nm, respectively.

Table I. EL performance of White TOLEDs using Al/ITO as the separating layer.

Item	Substrates Al/ITO(50 nm)/Al(x nm)/ITO (10 nm)	Voltage (V)	Lum. yield (cd/A)	CIE _{x,y}
1-1	2.5	9.75	0.47	(0.13, 0.11)
1-2	5	9.80	0.50	(0.14, 0.20)
1-3	7.5	8.24	0.76	(0.18, 0.32)
1-4	10	8.05	0.89	(0.30, 0.46)

* All device performance is measured at 100 mA/cm².

** Device structures of all items are the same. It is Al (100 nm)/ITO (50 nm)/Al (x nm)/ITO (10 nm)/CuPc (15 nm)/NPB (35 nm)/1.6%Rb@NPB (20 nm)/5%DSA-ph@ TBADN (20 nm)/Alq (20 nm)/Ca (5 nm)/Ag (15 nm).

4.2.4 Using Ni as the separating layer in a dual-cavity structure

Because Ni with higher work function can improve the ability of hole-injection, we also introduce Ni as the semi-transparent separating layer. We chose two thickness of Ni to change the ratio of light passage through these two cavities as we expect it is possible to obtain many colors of light by changing the ratio. Thus, we fabricated WTOLEDs with two different thickness of ITO and Ni as shown in Table II in which in items **2-1** to **2-9**, the thickness of ITO was varied from 10 to 180 nm but maintain the same thickness of Ni at 10 nm. Likewise, in items **2-10** to **2-13**, we increase the thickness of Ni to 20 nm.

EL spectra and 1931 CIE_{x,y} coordinates of items **2-1** to **2-9** are shown in Figure 4-6. It is observed that some devices have two emissive peak but others have only one. Because microcavity is affected by the cavity length and shows periodicity, we find that their EL spectra and 1931 CIE_{x,y} coordinates are changed also periodically with changing ITO thickness. Compared with CIE_{x,y} coordinates shown in Figure 4-6, a cycle of microcavity length is observed and appears around 120 nm of ITO.

In addition, we plot 1931 CIE_{x,y} coordinates of items **2-6** to **2-13** to examine the effect of the thickness of the separating layer, Ni. As shown in Figure 4-7, we found that with thickness of Ni increasing, the coordinate will be closer to the spectral region of yellow light. We think the increase of the thickness of Ni reduce the

transmittance itself and let most light resonate in the top-side cavity. As we mentioned in section 4.2.3, the top-side cavity emits yellow light, so the CIE_{x,y} coordinates of devices with 20 nm of Ni are closer to the area of yellow light than those with 10 nm of Ni.

Table II. EL characteristics of White TOLEDs using Ni as the separating layer.

Items	Substrates Al/ITO(x nm)/Ni(y nm)	Voltage (V)	Lum. yield (cd/A)	CIE _{x,y}
2-1	10 /10	9.85	2.06	(0.48, 0.47)
2-2	40 /10	8.87	0.45	(0.35, 0.35)
2-3	60 /10	8.89	0.62	(0.18, 0.21)
2-4	80 /10	8.19	1.40	(0.16, 0.43)
2-5	100/10	8.11	3.36	(0.28, 0.62)
2-6	120/10	9.25	2.02	(0.50,0.48)
2-7	140/10	8.97	1.13	(0.52,0.39)
2-8	160/10	11.01	0.20	(0.40,0.34)
2-9	180/10	9.80	0.29	(0.28,0.28)
2-10	120/20	8.86	2.86	(0.44,0.53)
2-11	140/20	9.18	1.26	(0.51,0.43)
2-12	160/20	9.67	0.48	(0.44,0.41)
2-13	180/20	9.75	1.09	(0.36,0.38)

* All device performance is measured at 100 mA/cm².

** Device structures of all items are the same. It is Al (100 nm)/ITO (x nm)/Ni (y nm)/CuPc (15 nm)/NPB (35 nm)/1.6%Rb@NPB (20 nm)/5%DSA-Ph@TBADN (20 nm)/Alq (20 nm)/Ca (5 nm)/Ag (15 nm).

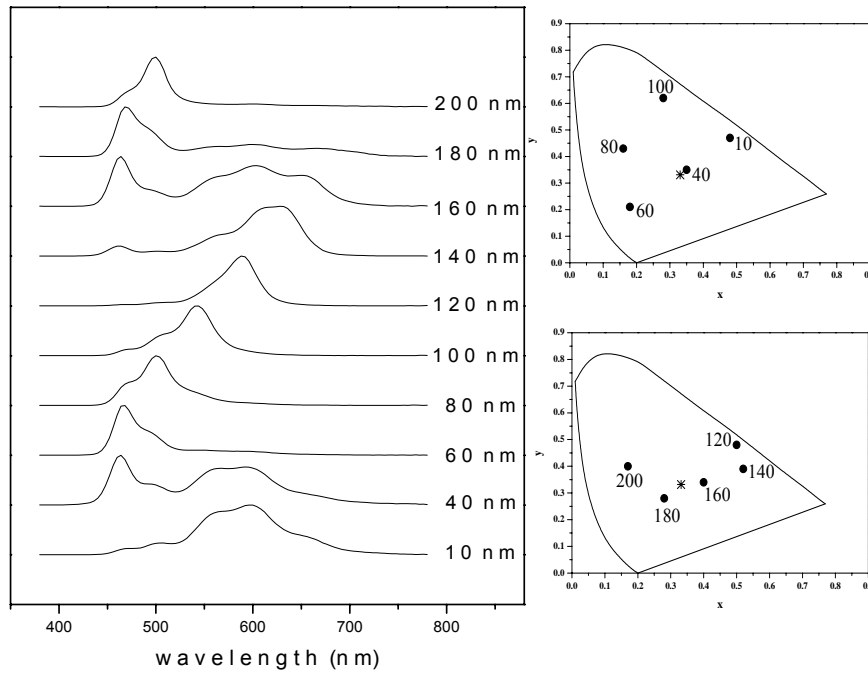


Figure 4-6 The EL spectra and 1931 $CIE_{x,y}$ diagram of dual-cavity white TOLED using Al (100 nm)/ITO and Ni (10 nm) as anode and separating layer, respectively. The thickness of ITO is 10, 40, 60, 80, 100, 120, 140, 160, 180 and 200 nm, respectively.

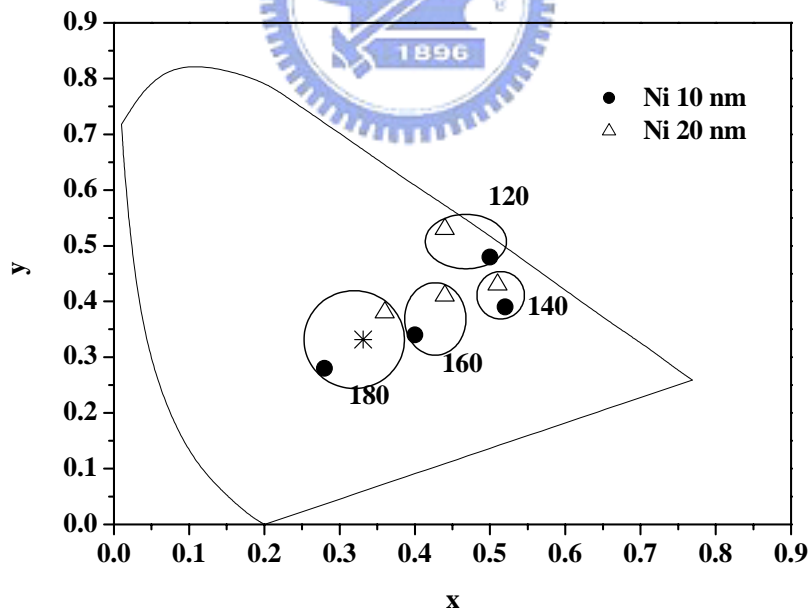


Figure 4-7 The EL spectra and 1931 $CIE_{x,y}$ diagram of dual-cavity white TOLED using Al(100 nm)/ITO and Ni as anode and separating layer, respectively. The thickness of ITO is 120, 140, 160 and 180 nm, respectively. In addition, the thickness of Ni is 10 and 20 nm, respectively.

One thing deserved to be mentioned is that the 1931 CIE_{x,y} coordinate of item **2-2** is (0.35, 0.35) which is very close to the ideal white color suggesting the construction of WTOLEDs are indeed possible by fine tuning the dual-cavity. The maximal luminance yield of 0.45 cd/A and a maximal luminance of 2300 cd/m² at 11.4 V can be achieved in our device, and the white color of item **2-2** device is quite stable under a wide range of drive current conditions. Figure 8 shows normalized EL spectral characteristics of the item **2-2** device. Slight abatement of the intensity of yellow light can also be observed with the CIE_{x,y} color coordinates shifted only from (0.35, 0.35) to (0.36, 0.35) when current density is increased from 10 to 700 mA/cm².

We have developed a white top emitting light-emitting device with a novel dual-cavity structure. Using different separating layer, we can tune the ratio of the blue and yellow emissions to achieve white emission. In Al/ITO/Ni device, we obtained a stable white emission even driven in high current density with CIE_{x,y} around (0.35, 0.35). A luminance efficiency of 0.45 cd/A and a maximal luminance of 2300 cd/m² at 11.4 V has been achieved.

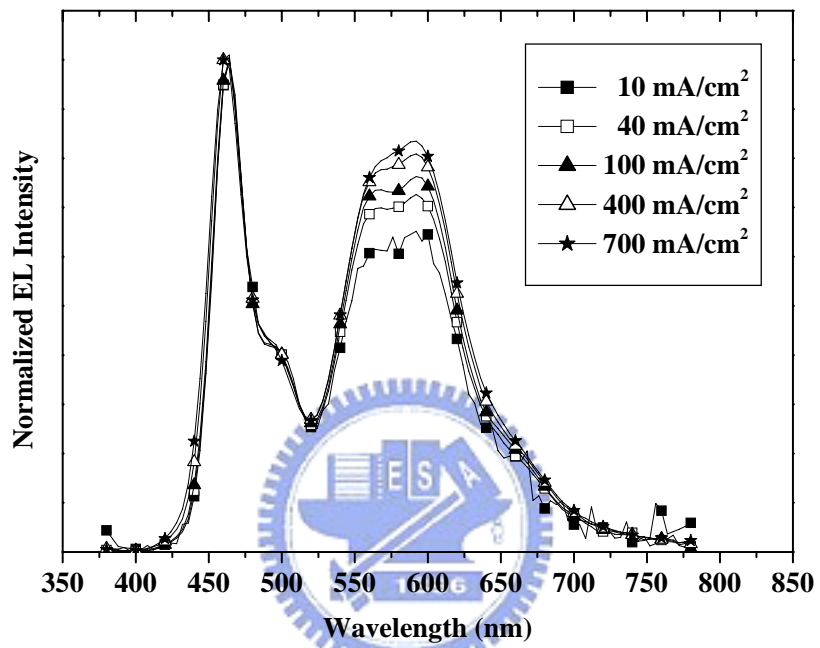


Figure 4-8 Normalized EL spectra of White TOLEDs of item 2-2, under different current density.

4.3 White light top-emitting organic light-emitting devices with a highly transparent cathode

Transmission of the metal cathode is considerably concerned in TOLEDs because of the nature of low transparency. In conventional top-emitting devices, two layer of Ca/Ag was used as transparent cathode (Figure 4-9), but low transmittance below 50 % of Ca/Ag cathode results in strong microcavity effect in the device.

White light always needs broad emission in visible region while spectral narrowing is most common phenomenon affected by microcavity effect. To alleviate the strong microcavity effect, we tried to use a highly transparent cathode. Metal-inorganic-metal (MIM) is widely used as low reflectance thin film. We insert a dielectric material, ZnSe, with high refraction index (~ 2.5) and high transparency. As shown in Figure 4-10, the transmittance of a multilayer cathode consists with Ca/ZnSe/Ag is much improved from Ca/Ag cathode. A maximum transparency of 70% can be achieved.

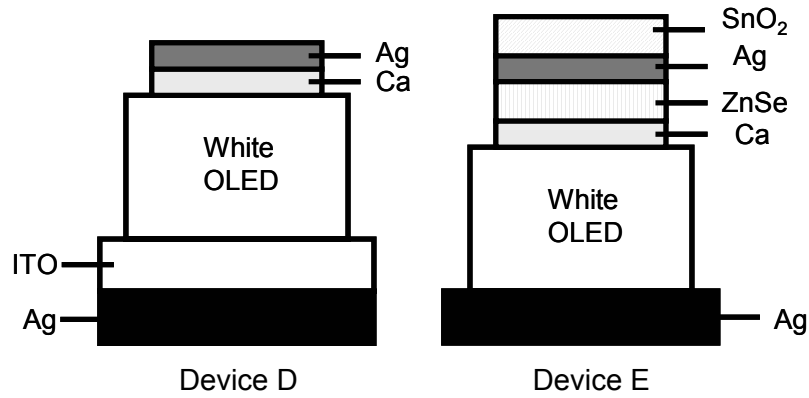


Figure 4-9 The device architecture of top-emitting devices.

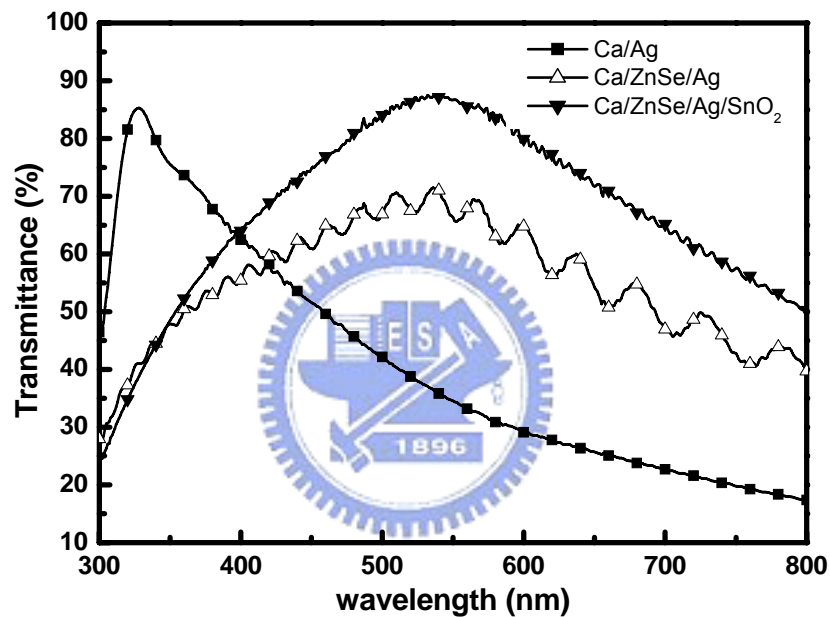


Figure 4-10 Transmittance spectra of Ca (5 nm)/Ag (15 nm), Ca/ZnSe (15 nm)/Ag and Ca/ZnSe (15 nm)/ Ag/ SnO₂ (22.5 nm) film.

Index-matching layer is another approach to improve transparency of the cathode [11]. High refractive index ($n \sim 2.0$) of SnO₂ was deposited onto multilayer cathode via thermal evaporation. A large improvement of transmittance can be observed in Figure 4-10. A maximum of $\sim 90\%$ transparency can be obtained and the region also agrees with our white light devices.

A multilayer cathode with high transparency was applied for white light devices. In top-emitting OLEDs, high reflectivity of the anode is also important for achieving high luminance efficiency. The good reflectivity of Ag and Al are most common used metal. In conventional top-emitting device, highly reflective metal combined with proper work function material (e.g. ITO) was often chosen as anode. However, larger optical length of the device could induce strong microcavity effect while the contribution of optical length is larger in ITO layer because of its larger refractive index ($n \sim 2.2$) than that of organic layer ($n \sim 1.6-1.7$). Furthermore, by direct photoionization measurements (Riken AC-2), the work function of Ag is found to be at 4.65 eV which is comparable to that of ITO. Consequently, to alleviate microcavity effect, the ITO layer should be eradicated, and the optical length of device can be efficiently shortened without sacrificing exciton confinement of the white emitter.

A multilayer cathode was evaluated with a device structure of Ag (200 nm)/CF_x/NPB (50 nm)/1.5 wt% Rubrene : NPB (20 nm)/3 DSA-Ph : MADN (40 nm)/Alq (10 nm)/Ca (5 nm)/ZnSe (15 nm)Ag (15 nm)/SnO₂ (22.5 nm)]. A conventional top-emitting device, Device **D**, with Ag/ITO as anode and Ca/Ag as cathode was also fabricated for comparison.

The detailed EL performances of these devices are summarized in Table III and their EL spectra are plotted in Figure 4-11. By observing the variation in the EL

spectra, we could understand more about microcavity effect caused in the device. It is apparent that most of light in Device **D** were whittled down owing to strong microcavity effect. A narrow spectrum exhibits peak wavelength at 468 nm with FWHM of 20 nm, and the efficiency of 0.6 cd/A with CIE coordinates (0.12, 0.17) was observed. Contrary to the device D, Device E with the multilayer cathode, a very broad white light emission with FWHM of 228 nm and a luminance yield of 1.7 cd/A with CIE coordinates (0.40, 0.41) was achieved. Viewing angle of these two devices was shown in Figure 4-12. Better viewing angle of the Device **E** also means microcavity effect has been alleviated in the top-emitting devices.

Color shift is also a serious issue in top-emitting light-emitting devices. EL spectra of cathode-modified white light TOLEDs with different viewing angle were shown in Figure 4-13. With increasing of viewing angle, EL spectra show blue shift. This is because the device is still affected by microcavity effect.

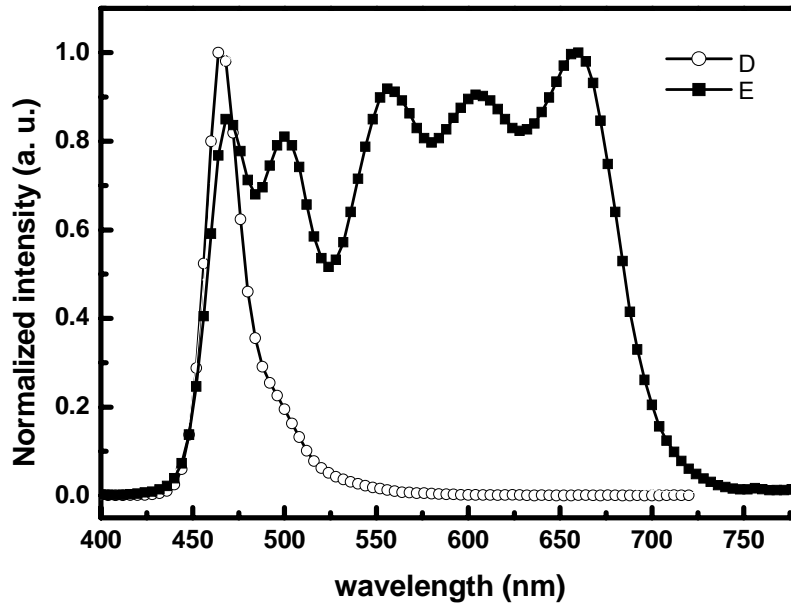


Figure 4-11 EL spectra of conventional TOLEDs and cathode-modified TOLEDs.

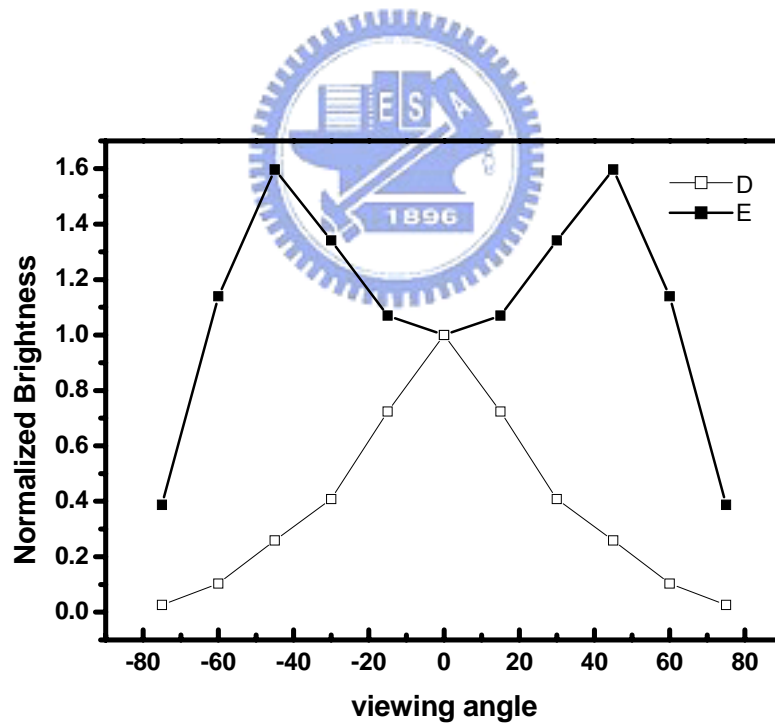


Figure 4-12 Viewing angle of conventional TOLEDs (D) and cathode-modified TOLEDs (E).

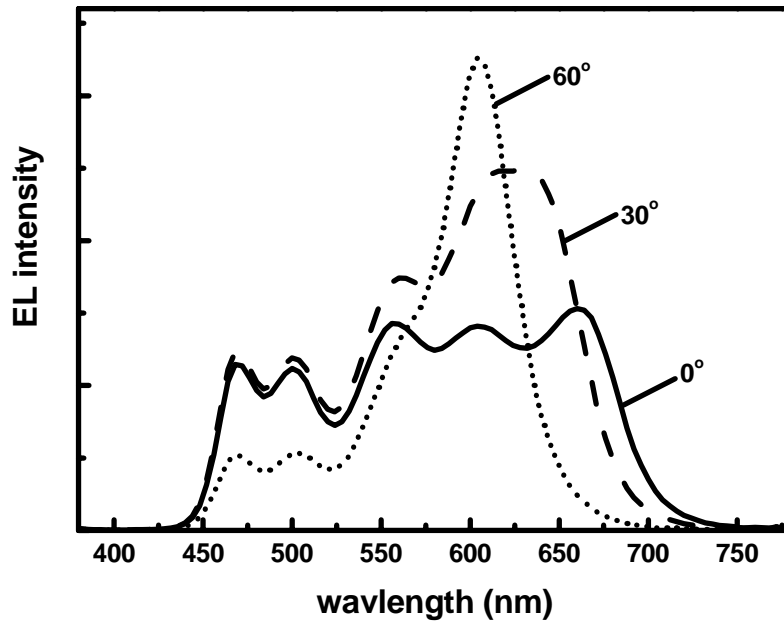


Figure 4-13 EL spectra of cathode-modified TOLEDs with different viewing angle.



RGB colors and intensity of the white light device coupled with color filter were also simulated and shown in Figures 4-14 and 4-15. A white emission with CIE coordinates of (0.363, 0.373) was obtained. Saturated colors from RGB pixels and NTSC ratio over 61% were also demonstrated. These properties show good potential for display application, however, the efficiency of the device need to be further improved.

Devices	WTOLEDs
R CIE _{x,y}	(0.664, 0.334)
G CIE _{x,y}	(0.313, 0.593)
B CIE _{x,y}	(0.112, 0.192)
W CIE _{x,y}	(0.363, 0.373)
NTSC ratio	61%

Figure 4-14 CIE colors and NTSC ratio simulation of three white light devices pass through color filter.

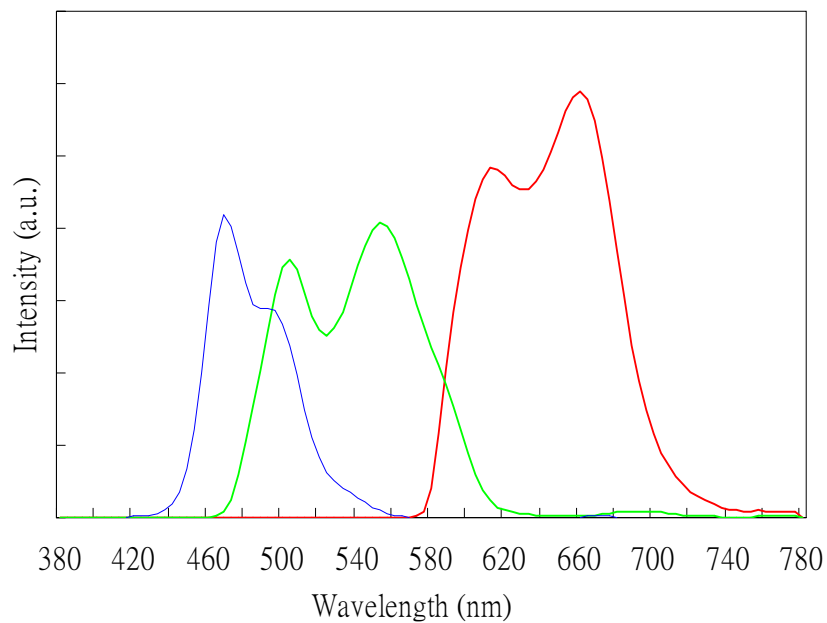


Figure 4-15 Intensity of RGB emission simulation of white light devices pass through color filter.

We demonstrated a white light TOLEDs with a very broad emission by introducing a highly transparent multilayer cathode. A device with FWHM of 228 nm and good CIE color coordinates of (0.40, 0.41) was achieved.

4.4 Highly efficient top-emitting white organic electroluminescent devices

To compare difference of the anode and the cathode, three device structures are designed and fabricated as shown in Figure 4-16. In Device **F**, the structure was [Ag (200 nm)/ITO (75 nm)/NPB (50 nm)/1.5 wt% rubrene : NPB (20 nm)/3 wt% DSA-Ph : 2-methyl-9,10-*di*(2-naphthyl)anthracene (MADN) (40 nm)/ Alq (10 nm)/Ca (5 nm)/Ag (15 nm)], which is the conventional white light top-emitting device. In Device **G**, ITO is the transparent anode, and cathode is the Ca (5 nm)/Ag (15 nm) capped with an index-matching layer of SnO₂ (22.5nm). The organic white emitter in device **G** is the same as in Device **F**. In Device **H**, we used 200 nm thick Ag as the reflective anode coated with a polymerized fluorocarbon film (CF_x) as the hole injection layer [12]. The cathode and organic white emitter were the same as Device **G**. Organic materials were deposited by thermal evaporation in an ULVAC Solciet OLED coater at a base vacuum of 10⁻⁷ Torr. All devices were hermetically sealed prior to testing. EL spectra, luminance yield, and CIE_{x,y} color coordinates were measured by a Photo Research PR-650 spectrophotometer driven by a programmable dc source.

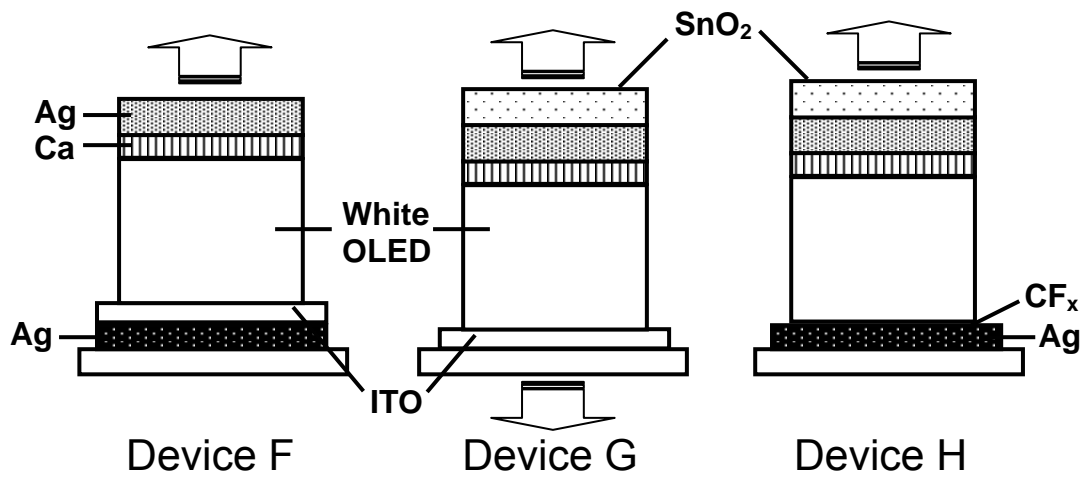


Figure 4-16 The device architecture of the three top-emitting devices, **F** (traditional), **G** (transparent), and **H** (electrode modified).

4.4.1 Device characteristics of WOLEDs

In top-emitting OLEDs, high reflectivity of the anode is important for achieving high luminance efficiency [13]. In our study, 200 nm Ag with a good reflectivity of more than 95% was used as the anode. Furthermore, by direct photoionization measurements (Riken AC-2), the work function of Ag is found to be at 4.65 eV which is comparable to that of ITO, like CF_x, is overcoated onto the Ag surface to further improve its hole injection.

Figure 4-17 shows the transmission spectrum of Ca/Ag cathode capped with different thicknesses of SnO₂ varying between 7.5, 15, 22.5, and 30 nm. We realize that the transmission of a metal cathode is a critical issue to be addressed in TOLEDs

because of its nature of low transparency. In order to improve the transparency of the cathode, a high refractive index ($n \sim 2.0$) of SnO_2 was deposited via thermal evaporation. With increasing thickness of SnO_2 , the wavelength with optimal transmittance is shifted gradually from the blue to red region. Here, 22.5 nm thick SnO_2 was selected due to its higher transparency throughout the entire visible region of our *broad* white emitter.

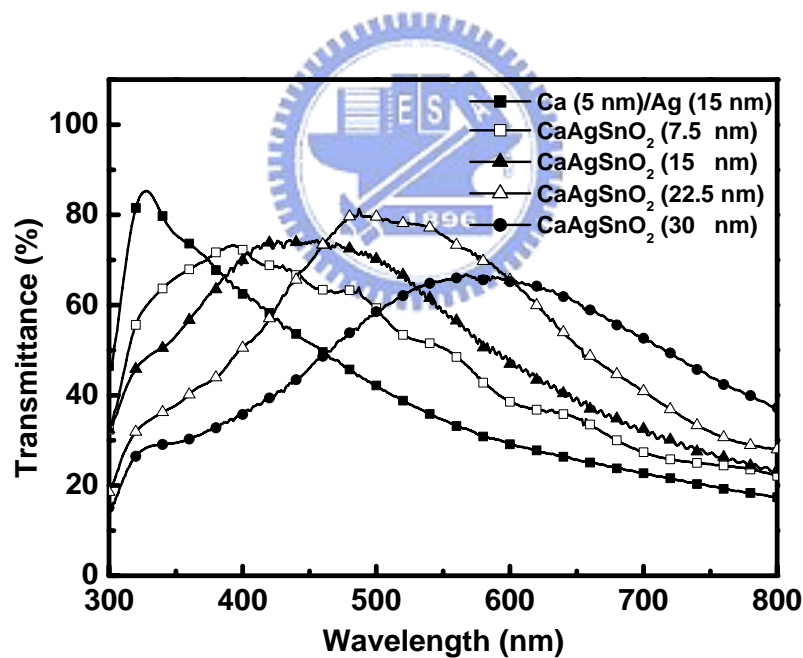
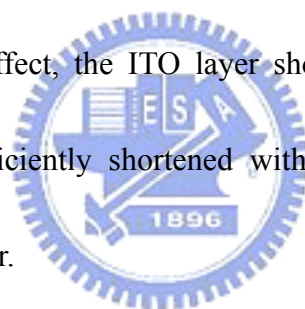


Figure 4-17 Transmittance of Ca (5 nm)/Ag (15 nm) cathode capped with different thicknesses of SnO_2 .

The detailed EL performances of these devices are summarized in Table IV and their EL spectra are plotted in Figure 4-18. By observing the variation in the EL spectra, we can analyze and understand more about the microcavity effect caused by

the device structure. It is apparent that most of white light generated in Device **F** was whittled down and showed that a narrow spectrum exhibits a peak wavelength at 468 nm with a FWHM of 20 nm. Saturated color with CIE_{x,y} coordinates (0.12, 0.17) and low efficiency of 0.6 cd/A were observed. Although metal/ITO was often chosen as the anode in conventional top-emitting devices [10], the contribution of optical length is larger in the ITO layer ($n \sim 2.2$) than that of organic layer ($n \sim 1.6-1.7$), and a longer optical length tends to lead to a stronger microcavity effect in Device **F**. To alleviate this unwanted microcavity effect, the ITO layer should be eradicated, and optical length of device can be efficiently shortened without altering the recombination region within the white emitter.



Contrary to Device **F**, a large fraction of yellow light is “detrapped” in Devices **G** and **H**. It evidently suggests that successful alleviation of microcavity effect can extract some more yellow emission and enhance EL intensity. This enhancement also agrees with the improved transmission of the multilayer cathode. In the transparent Device **B**, a luminance yield of 2.7 cd/A was achieved from the top side but with more than 70% of light emitted from ITO anode (bottom side). The high reflectance Ag anode of Device **H** forces white light to emit from the top semitransparent cathode thus leading to the very high efficiency of 22.2 cd/A (9.6 lm/W). We believe this

significant enhancement in efficiency can be attributed to the combined effect of successful attenuation of the adverse microcavity effect and the improvement of light outcoupling with index matching material [10, 14]. A broad white-light emission with a FWHM of 136 nm generated from Device **H** is also wider than that of bottom-emitting device (116 nm). Although Device **H** is a broadband-emitting device, it does not have a very good white color. A near white-light emission of CIE coordinates of $(x=0.31, y=0.47)$ was achieved which is also comparable to that of bottom-emitting device $(x=0.27, y=0.40)$. We believe the color of the white device can be further improved by selecting a proper set of emitting materials.

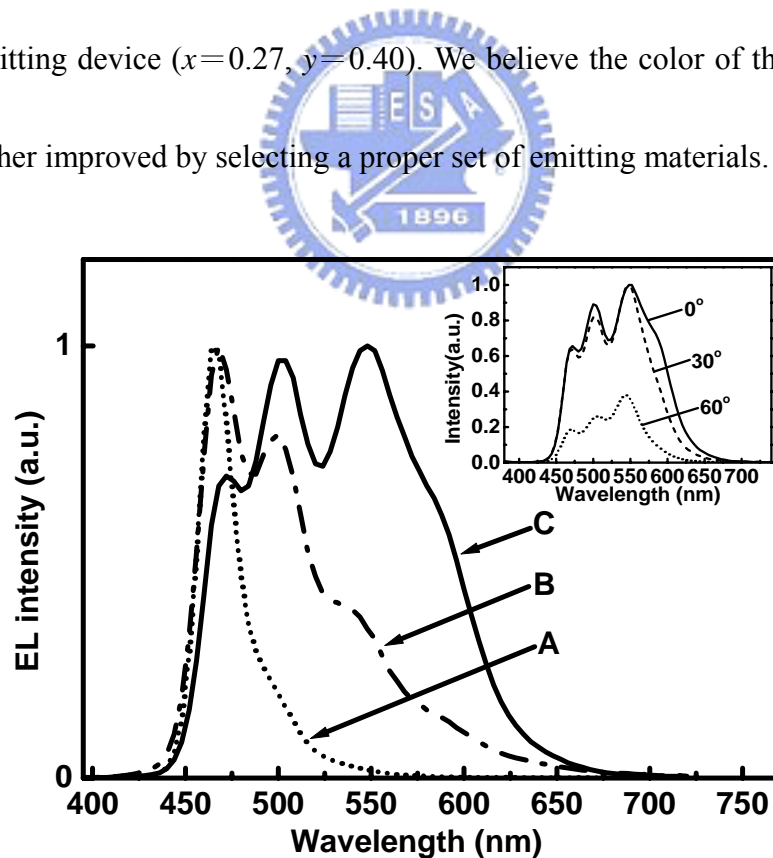


Figure 4-18 EL spectra of the three top-emitting devices. Insert: EL spectra of Device **H** under viewing angles of 0° , 30° and 60° off the surface normal.

Table IV. EL performance of Devices **F**, **G**, and **H** measured at 20 mA/cm².

Devices	Voltage (V)	Lum. yield (cd/A)	Efficiency (lm/W)	CIE (x,y)	FWHM (nm)
F	5.3	0.6	0.4	0.12, 0.17	20
G (top)	6.6	2.7	1.3	0.21, 0.35	64
G (bottom)	6.6	6.6	3.1	0.27, 0.40	116
H	7.3	22.2	9.6	0.31, 0.47	136

The EL spectra of Device **H** under different viewing angles of 0°, 30° and 60° were shown in Figure 4-18. In a strong microcavity device, with increasing viewing angle, the peak wavelength shifts rapidly to a shorter wavelength and the intensity decreases. It is to be noted that the emission shows less angular dependence in Device **H** as three main peaks of white emission at different viewing angles remain the same.

Current density-voltage (*J-V*) and brightness-voltage (*B-V*) curves of these three devices are shown in Figs. 4-19 (a) and (b), respectively. It is noteworthy that both *J-V* and *B-V* curves of Device **H** show the steepest response. At a high current density of 300 mA/cm², brightness over 57 000 cd/m² was achieved at 10 V which further implies good electron and hole balance in the new top-emitting device was also achieved at the same time.

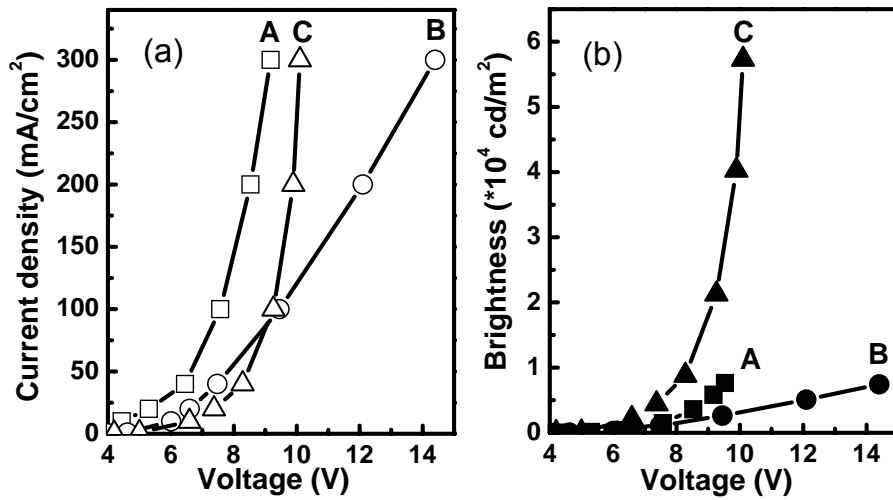


Figure 4-19 (a) *J-V* characteristics and (b) *B-V* characteristics of Devices F, G, and H.

4.4.2 WOLEDs on TFT array

The top-emitting WOLED structure was integrated with a 1.3" QCIF LTPS-TFT substrate. Figure 4-20 shows the photo images of the panel fabricated with a Cr anode and a Ca/Ag/SnO₂ cathode. It is to be noted that there is no significant color shift of the device at different viewing angle, as shown in Figure 4-21. The white light emission with CIE coordinates of (0.29, 0.40) was obtained by using three-component emitters to enhance RGB saturation. The simulation after coupled with color filter reveals that the color gamut is increased from 55% to 63%.

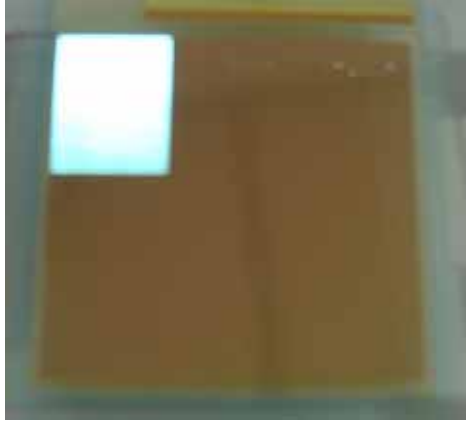


Figure 4-20 Photo of white light top-emitting OLED on LTPS-TFT backplane.

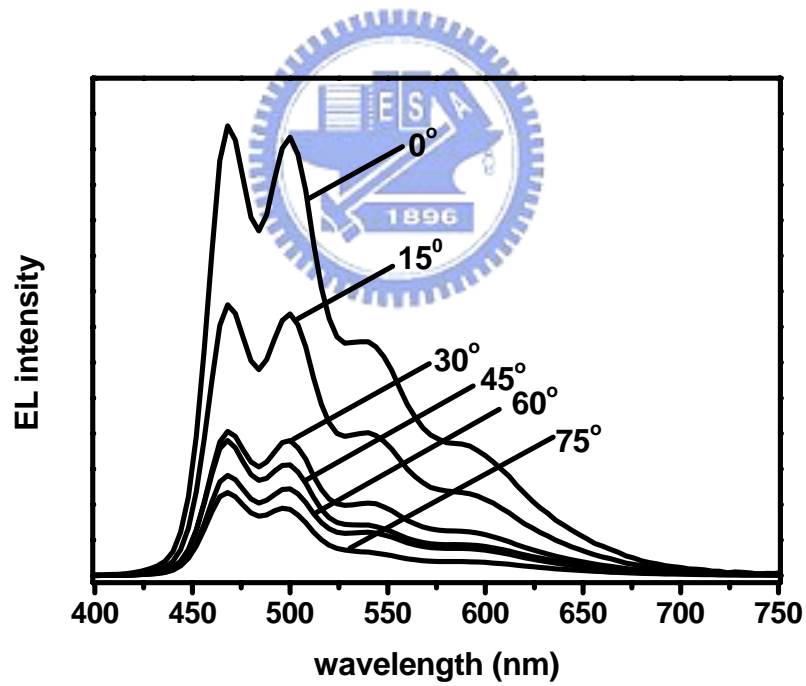


Figure 4-21 EL spectra of the white light panel at different viewing angle.

References

- [1] C. W. Tang and S. A. VanSlyke, *Appl. Phys. Lett.* **51** (1987) 913.
- [2] K. Mameno, S. Matsumoto, R. Nishikawa, T. Sasatani, K. Suzuki, T. Yamaguchi, K. Yoneda, Y. Hamada and N. Saito, *Proceedings of The 10th International Display Workshops*, 267, Fukouka, Japan (2003).
- [3] M. Kashiwabara, K. Hanawa, R. Asaki, I. Kobori, R. Matsuura, H. Yamada, T. Yamamoto, A. Ozawa, Y. Sato, S. Terada, J. Yamada, T. Sasaoka, S. Tamura and T. Urabe, *SID 04 Digest*, 1017 (2004).
- [4] A. Dodabalapur, L. J. Rothberg, R. H. Jordan, T. M. Miller, R. E. Slusher, and J. . Phillips, *J. Appl. Phys.* **80** (1996) 6954.
- [5] E. F. Schubert; N. E. J. Hunt; M. Micovic; R. J. Malik; D. L. Sivco; A. Y. Cho; G. J. Zydzik, *Science* **265** (1994) 943.
- [6] A. Dodabalapur, L. J. Rothberg, T. M. Miller, and E. W. Kwock, *Appl. Phys. Lett.* **64** (1994) 2486.
- [7] B. Balaganesan, W. J. Shen, and C. H. Chen, *Tetrahedron Lett.* **44** (2003) 5747.
- [8] Hatwar, Tukaram Kisan, EP 1 286 569 A1, (2003).
- [9] I. M. Chen, T. Y. Hsu and Franklin C. Hong, *Appl. Phys. Lett.* **81** (2002) 1899.
- [10] A. Dodabalapur, L. J. Rothberg, and T. M. Miller *Electron. Lett.* **30** (1994) 1000.
- [11] L. S. Hung, C. W. Tang, M. G. Mason, P. Raychaudhuri, and J. Madathil, *Appl.*

Phys. Lett. **78** (2001) 544.

[12] L. S. Hung, L. R. Zheng, and M. G. Mason, *Appl. Phys. Lett.* **78** (2001) 673.

[13] C.-W. Chen, P.-Y. Hsieh, H.-H. Chiang, C.-L. Lin, H.-M. Wu, and C.-C. Wu,

Appl. Phys. Lett. **83** (2003) 5127.

[14] H. Riel, S. Karg, T. Beierlein, W. Rieß, and K. Neyts, *J. Appl. Phys.* **94** (2003)


5290.



Chapter 5

High-efficiency and easily manufactured top-emitting white organic electroluminescent devices

5.1 WTOLEDs with a single blue dopant



Device fabrication of white-light top-emitting light-emitting devices was further simplified by using a single blue dopant. In a common white light OLEDs, more than two emissive dopants will be utilized to mix a white emission. In a top-emitting device, it is easy to adjust optical length to tune the resonance wavelength at certain region due to the cavity effect. In this chapter, we alleviate undesired cavity effect in the device to achieve broad white-emission. At the same time, we introduce a single blue dopant and enhance yellow emission by tuning optical length of the device to generate white emission.

Figure 5-1 shows the EL spectrum of blue emitter, DSA-Ph. Because of the *residual of Alq emission*, blue devices always suffer the issue of poor color saturation.

However, taking a close look of the spectrum, impure emission from Alq around 525-575 nm happened to show the similar spectrum like rubrene. We try to accomplish an ideal of adjusting the cavity effect in the device to enhance the intensity of yellow emission. As a result, we can achieve a broad white-emission.

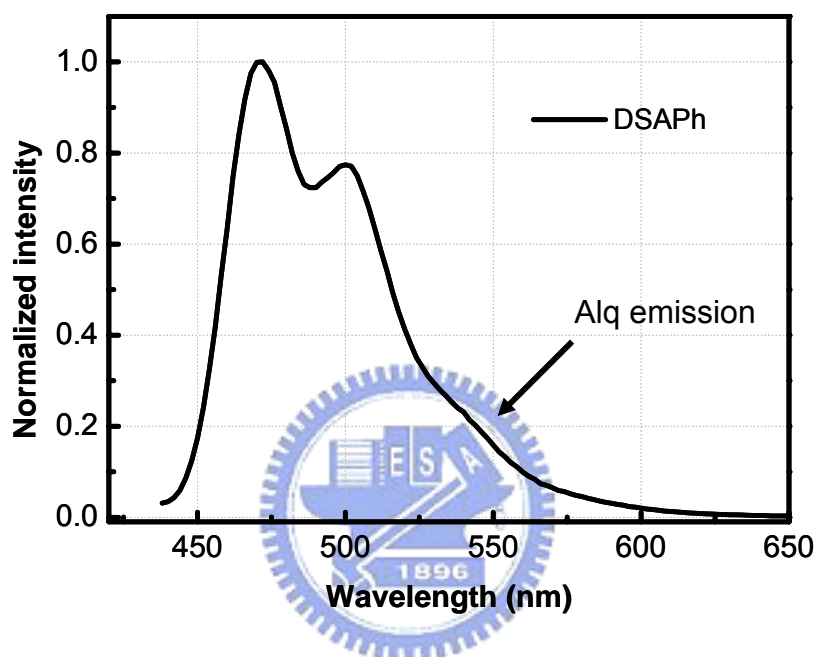


Figure 5-1 The EL spectrum of the blue emitter, DSAPh.

The device structure of top-emitting devices are designed and fabricated as shown in Figure 5-2. 200-nm-thick Ag as reflective anode coated with a polymerized fluorocarbon film (CF_x) as hole injection layer were used and cathode is Ca (5 nm)/Ag (15 nm) capped with an index-matching layer of SnO_2 (22.5 nm). A blue organic emitter of DSA-Ph doped in MAND was utilized for white light emission. With fixed EML and ETL of MADN: 3%DSAPh (30 nm) and Alq (30 nm), we varied

thickness of NPB from 30 to 45 nm. A common bottom-emitting device was also compared [1].

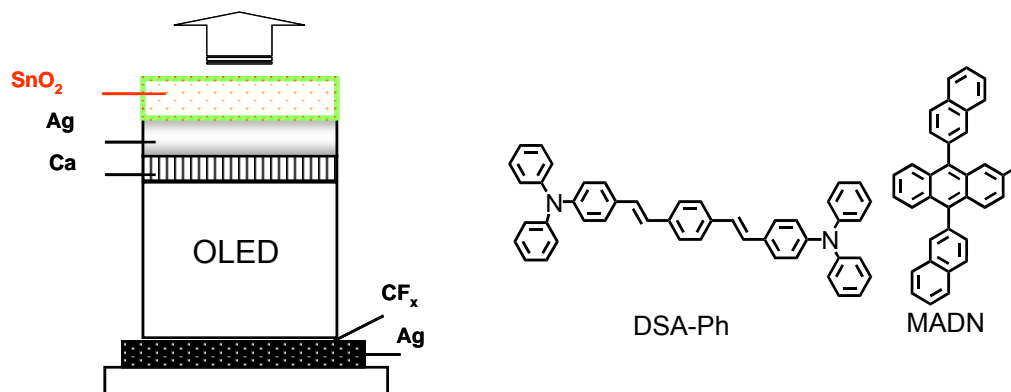
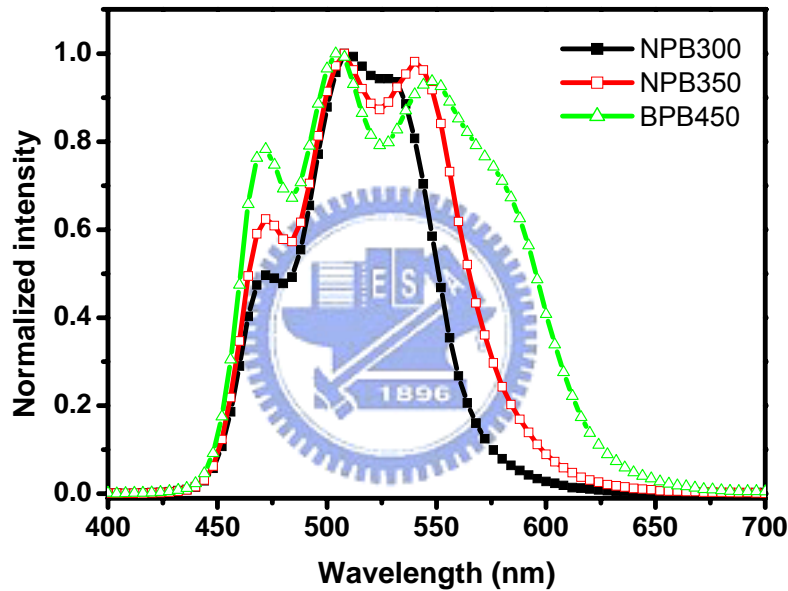


Figure 5-2 Chemical structures of key materials used in this study and device architecture of the three top-emitting devices.

The detailed EL performances of these devices and their EL spectra are plotted in Figures 5-3 and 5-4. In the bottom-emitting device, blue emission from Alq was observed with a device structure of ITO/NPB/EML/Alq/LiF/Al. A efficiency of 9.7 cd/A at 20 mA/cm² and 5.7 V with a CIE coordinated of (0.16, 0.32) was achieved. We utilized this impure emission and further tune optical length in the device to enhance emission around 520-600 nm range to generate a white light.

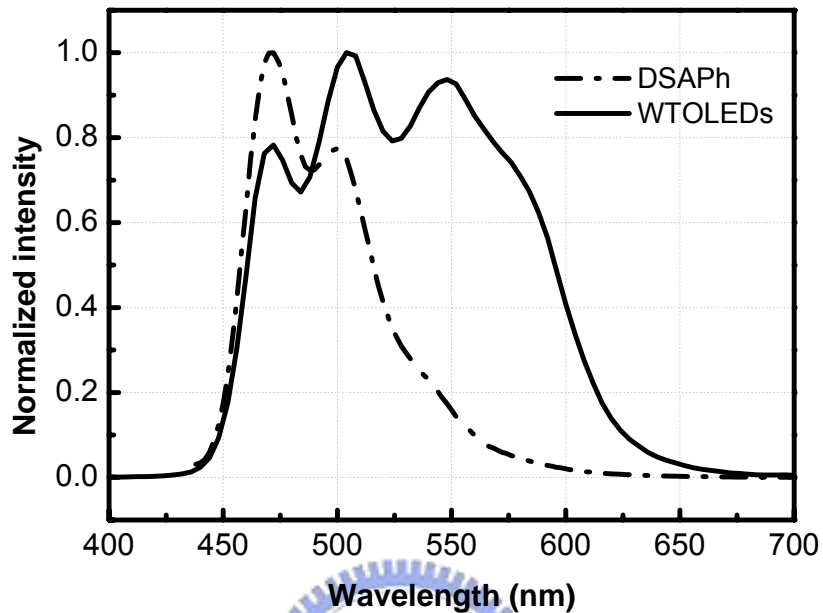
With NPB thickness of 45 nm, a very broad white-light emission with FWHM of 132 nm was achieved. It evidently shows that successful optimization of microcavity effect to enhance yellow light to achieve white light in the top-emitting device. A

device with the high EL efficiency of 12.5 cd/A at 20 mA/cm² and 7.9 V with Commission Internationale d'Eclairage (CIE) coordinates of (x = 0.30, y = 0.47) has been demonstrated. To the best of our knowledge, this is the first high efficient *broadband* white light emissions using a *single* blue dopant ever reported in a top-emitting device.



Devices	Voltage (V)	Yield (cd/A)	CIE (x,y)	Wavelength (nm)	FWHM (nm)
NPB300	7.7	16.0	0.17, 0.53	508	64
NPB350	7.8	16.1	0.22, 0.52	508	104
NPB450	7.9	12.5	0.30, 0.47	504	132

Figure 5-3 EL spectra and device performance of WTOLEDs with different thicknesses of NPB.



Devices	Voltage (V)	Lum. Yield (cd/A)	Efficiency (lm/W)	CIE (x,y)	FWHM (nm)
Bottom	5.7	9.7	5.5	0.16, 0.32	60
WTOLEDs	7.9	12.5	5	0.30, 0.47	132

Figure 5-4 EL spectra and performance comparisons of WTOLEDs and DSAPh doped bottom-emitting device.

Devices with the similar optical length were fabricated to achieve higher efficiency. We have introduced a composite hole-transporting layer (c-HTL) consisting of 50% CuPc and 50% NPB [2], 4,4',4''-tris[2-naphthyl (phenyl)-amino] triphenylamine (2-TNATA), and EHI-608 doped F4-TCNQ layer. The EL spectra of three devices were plotted in Figures 5-5, 5-6 and 5-7 and the detailed EL

performance were listed in Table I. Although an additional layer of hole-injection layer didn't improve device efficiency, we can observe the optical interference in the device. The resonance wavelength of the devices was increased with the increasing optical length of the device. Compared with 45 nm-thick NPB and c-HTL (20 nm)/NPB (15 and 20 nm) devices, all of the three devices have similar EL spectra. As we know, c-HTL impedes hole injection leads to the higher driving voltage. That also implies that lower hole-injection property alter the emission combination zone of the devices. The effect of the shift of the emission dipole was compensated by thickness of the organic layer. Similar phenomena were observed in 2-TNATA and EHI-608 doped F4-TCNQ devices. 2-TNATA, EHI-608 and F4-TCNQ were purchased from e-Ray optoelectronics. Both of the two HTL were improved hole injection. Compared with total thickness of 45 nm of NPB, 2-TNATA, and EHI-608 doped F4-TCNQ devices, the resonance wavelength were exhibited at 550, 584, and 612 nm, respectively. The stronger hole-injection layer leads to more red shift of resonance wavelength of the devices. The device with longer resonance wavelength at red region can achieve better chromaticity in white light. The EHI-608 doped F4-TCNQ device shows better CIE color of (0.37, 0.41). However, large color shift from the original blue emission results in lower efficiency. The efficiency of the device is only 5 cd/A.

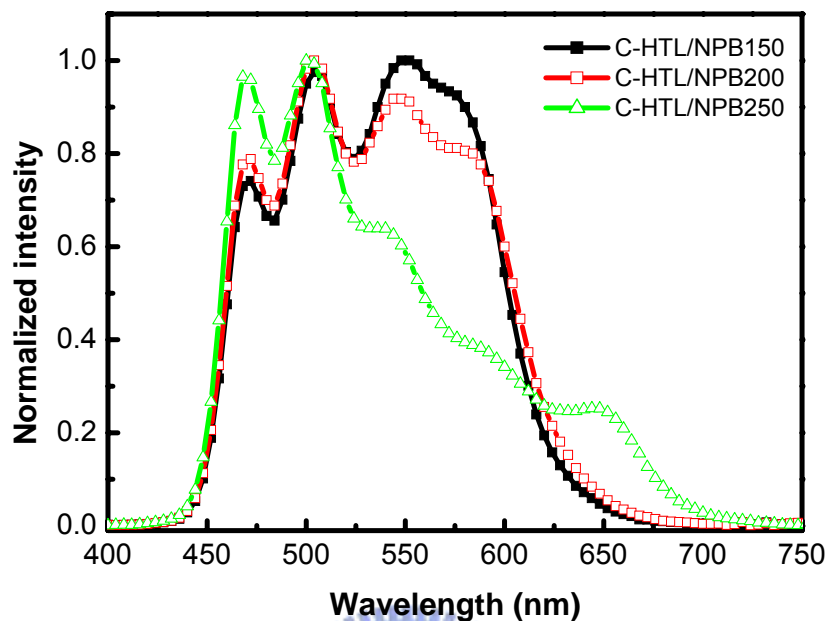


Figure 5-5 EL spectra of WTOLEDs with the structure of c-HTL(20 nm)/NPB (vary)/EML (30 nm)/Alq (30 nm)/Ca/Ag/SnO₂.

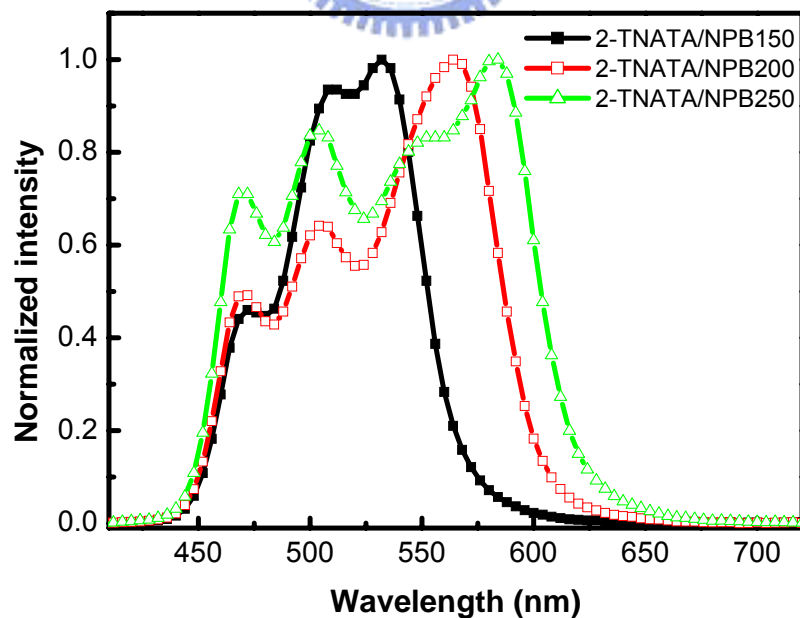


Figure 5-6 EL spectra EL spectra of WTOLEDs with the structure of 2-TNATA (20 nm)/NPB (vary)/EML (30 nm)/Alq (30 nm)/Ca/Ag/SnO₂.

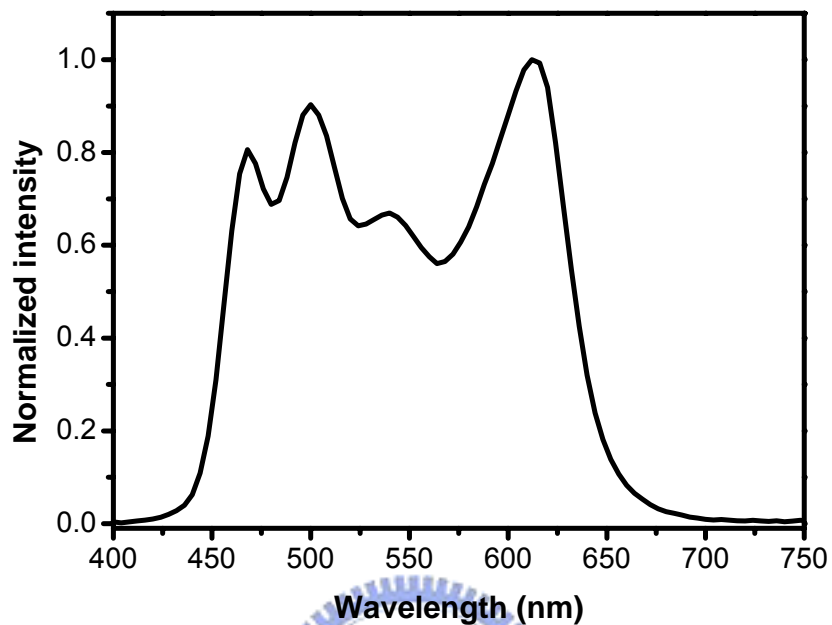


Figure 5-7 EL spectra of WTOLEDs with the structure of 608: F4-TCNQ (20 nm)/NPB (25 nm)/EML (30 nm)/Alq (20 nm)/Alq: Cs₂CO₃ (10 nm)/Ag/SnO₂.

Table I. EL performance of devices measured at 20 mA/cm².

Devices	Voltage (V)	Yield (cd/A)	CIEx,y	Wavelength (nm)	FWHM (nm)
NPB450	7.9	12.5	0.30, 0.48	504	132
C-HTL200/NPB200	8.9	7.0	0.32, 0.46	504	144
C-HTL200/NPB250	10.1	4.2	0.28, 0.41	504	144
2-TNATA200/NPB250	7.0	10.7	0.33, 0.46	584	140
EHI608200/NPB250	7.3	5.0	0.37, 0.41	612	176

5.2 WTOLEDs with a stacked structure

Recently, a high-efficiency OLED with multiple emission units stacked in series has been demonstrated [3, 4]. This tandem OLEDs exhibit the improved efficiency that scales roughly linearly with the number of emission units. To obtain high-efficiency WTOLEDs, we combined two technologies of top emission and tandem OLEDs. Two emission units were connected by WO_3 [5].

The detailed device structure and thicknesses of layers were shown in figure 5-8. Two emission units with the structure of EHI-608:2% F4-TCNQ (25 nm)/NPB (20 nm)/MADN: 3 % DSAPh (30 nm)/Alq (20 nm)/Alq: 2% Cs_2CO_3 (10 nm) were connected with 5 nm of WO_3 . EL spectra are plotted in Figures 5-9 and the device performances were shown in figure 5-10. Although a very high efficiency of 30 cd/A was obtained, the CIE color coordinates of the device were (0.260, 0.608). A very sharp emission exhibits at the wavelength of 550 nm was observed. As we mentioned in chapter 4, the longer optical length of the device will induce stronger microcavity effect. To solve the intrinsically thick device structure in a tandem OLED and further alleviate microcavity in a top-emitting structure will be another challenge to overcome. On the other hand, development of transparent ITO electrode without sputtering damage is also very important.

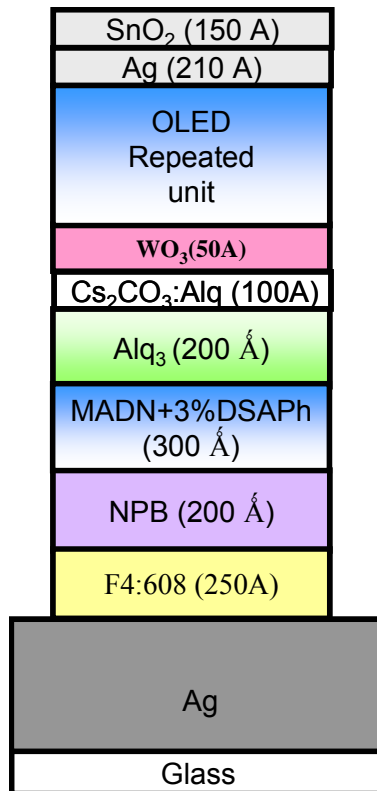


Figure 5-8 Device structure of tandem WTOLEDs.

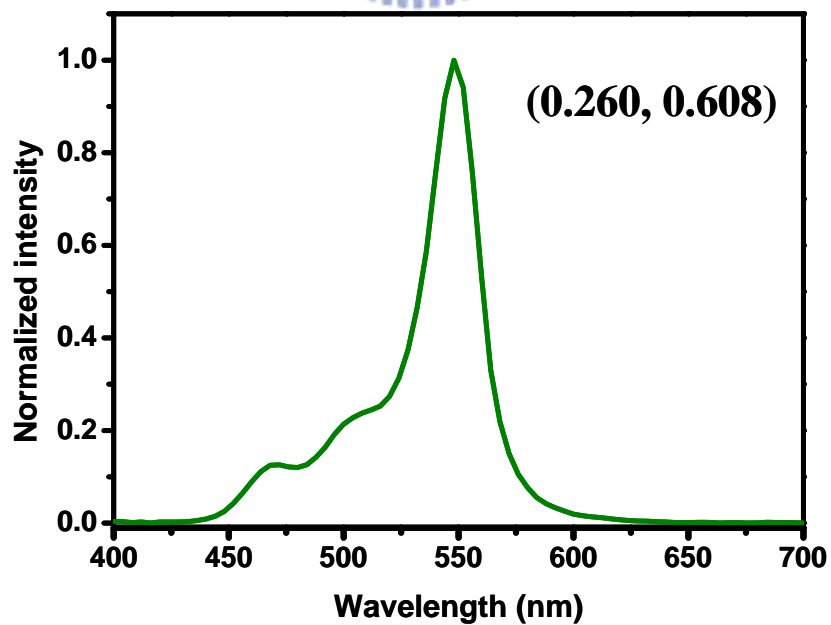


Figure 5-9 EL spectra of tandem WTOLEDs.

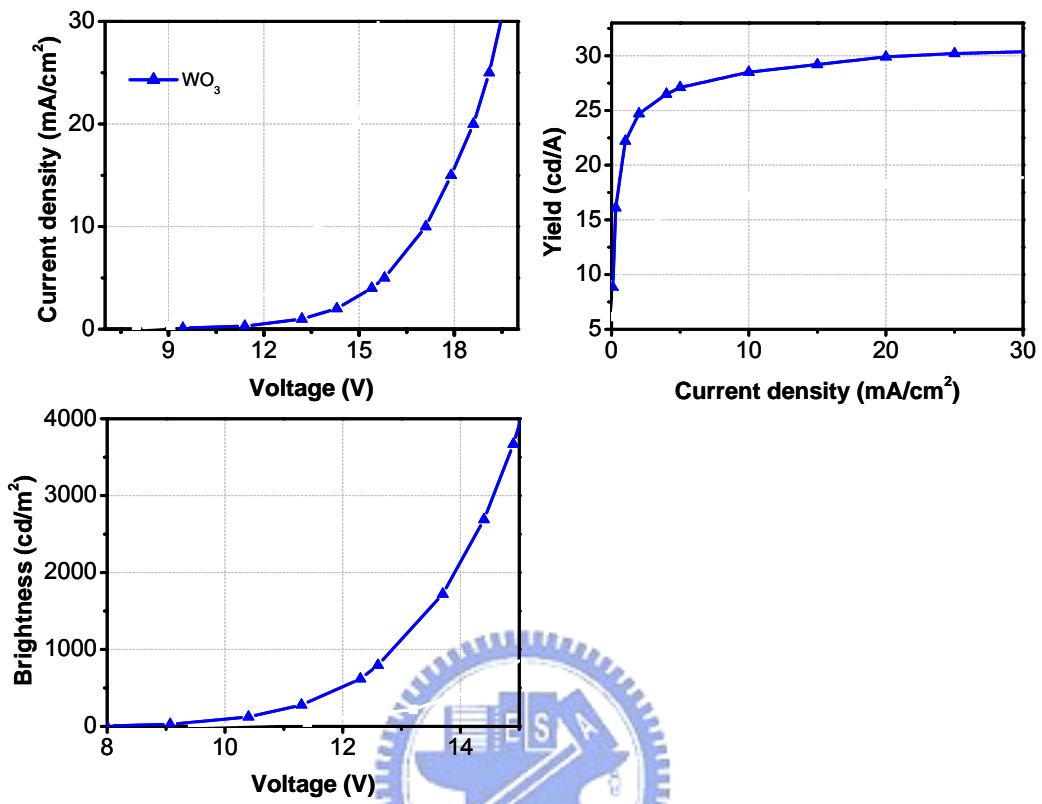


Figure 5-10 EL performance of tandem WTOLEDs.

Reference

- [1] M. T. Lee, H. H. Chen, C. H. Liao, C. H. Tsai and C. H. Chen, *Appl. Phys. Lett.* **85**, (2004) 3301.
- [2] C. H. Liao, M. T. Lee, and C. H. Tsai and C. H. Chen, *Appl. Phys. Lett.* **86** (2005) 203507.
- [3] T. Matsumoto, T. Nakada, J. Endo, K. Mori, N. Kavamura, A. Yokoi, and J. Kido, *SID 03 Digest*, 979 (2004).
- [4] L. S. Liao, K. P. Klubek, and C. W. Tang, *Appl. Phys. Lett.* **84** (2004) 167.
- [5] C. C. Chang, S.-W. Hwang, C. H. Chen and J.-F. Chen, *Appl. Phys. Lett.* **87** (2005) 253501.

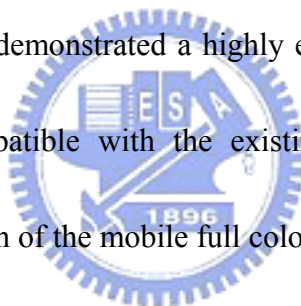


Chapter 6

Summary and future prospects

6.1 Summary

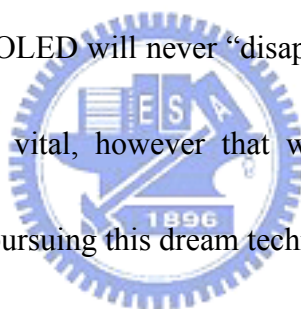
RGB TOLEDs provide larger AR, longer lifetime, higher efficiency, lower power consumption and better color saturation than those of the conventional bottom-emitting devices. We demonstrated a highly efficient RGB TOLED structure that is expected to be compatible with the existing manufacturing process and expedite the commercialization of the mobile full color AMOLEDs.



We have also introduced a high-efficiency white TOLED with a modified anode and cathode. Shortening the optical length of the device alleviates the adverse microcavity effect from which a broad emission of white light is obtained. We believe this highly efficient white top-emitting device may provide a possible solution for the manufacturing the next generation of high-resolution full color LTPS-TFT AMOLED displays.

6.2 Future prospects

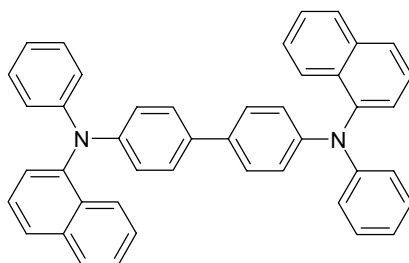
In 2004-2006, three full-color AMOLED displays have been commercialized. There is no doubt that OLED is the best display technology in the world. Unfortunately, we are facing a huge obstacle in increasing public awareness that OLED is the best. That's not because the intrinsic property of the OLED is not good enough but because people are not fully convinced that OLED business can make money. The answer is not "YES" or "NO" but rather "WHEN" and "HOW"?. However, it is not that clear answer is in sight. Many people working in the field including myself believe that OLED will never "disappear" as it is truly "the ultimate display" for the future. It is vital, however that we OLEDers should always be enthusiastic and persistent in pursuing this dream technology.



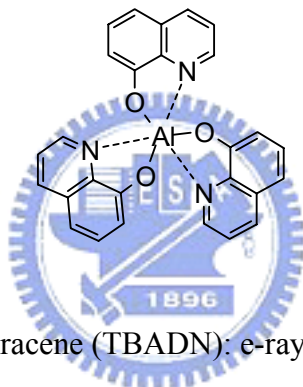
In the development of human history, we keep seeking to experience the "new experiences", satisfy their desires and establish values. I believe this need will not be satisfied by the images displayed by current display technology forever. For the time being, our small contribution unfortunately is neither sufficient nor punctual. We should continually work hard to do R&D and to build up infra-structure and supply chain, and to achieve cost down in manufacturing of OLED. Maybe, only then we can realize a future where life is really "*Bright*" and in "*Full colors*"!

Materials

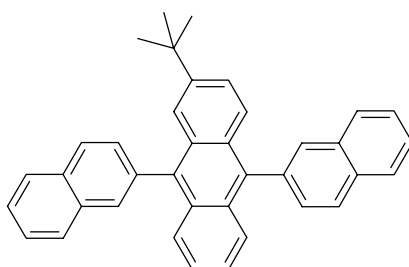
4,4'-bis[*N*-(1-naphthyl)-*N*-phenyl-amino]biphenyl (NPB): e-ray optoelectronics



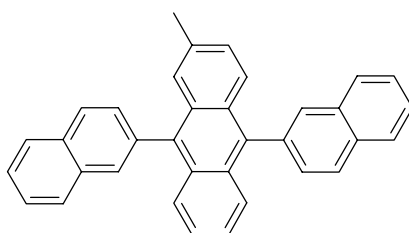
Aluminum *tris*(8-hydroxyquinoline) (Alq): e-ray optoelectronics



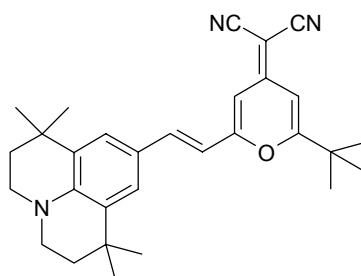
2-(*t*-butyl) *di*-(2-naphthyl)anthracene (TBADN): e-ray optoelectronics



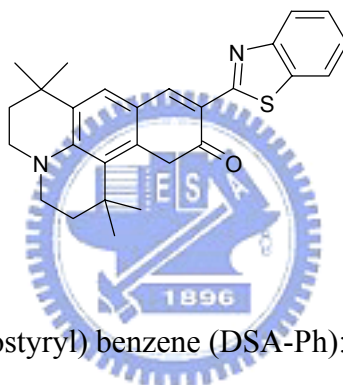
2-methyl-9,10-*di*(2-naphthyl)anthracene (MADN): e-ray optoelectronics



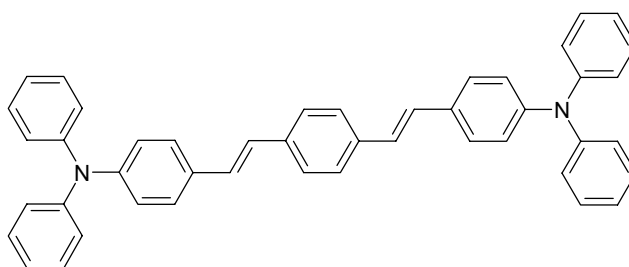
2-{2-(t-butyl)-6-[(E)-2-(1,1,7,7-tetramethyl-2,3,6,7-tetrahydro-1H,5H-pyrido [3,2,1-ij] quinoline-9-yl)-1-ethenyl]-4H-4-pyraniden}malonitrile (DCJTb): e-ray optoelectronics



10-(1,3-benzothiazol-2-yl)-1,1,7,7-tetramethyl-2,3,6,7-tetrahydro-1H,5H,11H-pyrano[2,3-f]pyrido [3,2,1-ij]quinoline-11-one (C-545T): e-ray optoelectronics



p-bis(p-N,N-di-phenyl-aminostyryl) benzene (DSA-Ph): e-ray optoelectronics



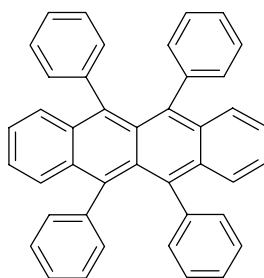
ER33: e-ray optoelectronics' proprietary

EB512: e-ray optoelectronics' proprietary

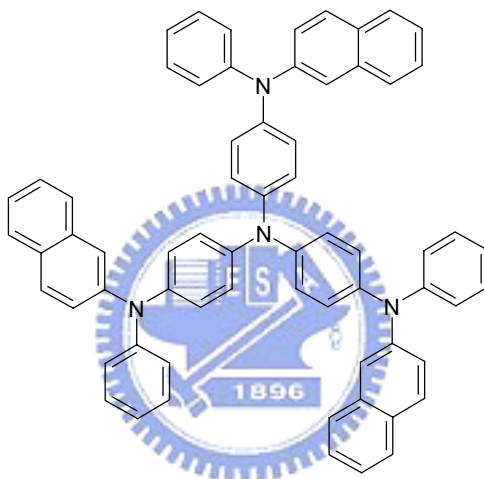
EB46: e-ray optoelectronics' proprietary

EHI-608: e-ray optoelectronics' proprietary

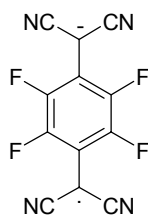
5,6,11,12-tetraphenylnaphthacene (Rubrene): e-ray optoelectronics



4,4',4''-tris[2-naphthyl (phenyl)-amino] triphenylamine (2-TNATA): e-ray optoelectronics



Tetra(fluoro)-tetra(cyano)quiondimethane (F4-TCNQ): e-ray optoelectronics



Calcium: Stern; 99%

Sliver: Stern; 99.99%

LiF: Aldrich; 99.99%

Aluminum: Aldrich; 99.999%

Cs₂CO₃: Aldrich; 99.994%

SnO₂: Stern; 99.5%

ZnSe: Stern; 99.5%

Publication List

A. Journal Papers

1. S. F. Hsu, C. C. Lee, A. T. Hu and C. H. Chen, “Fabrication of blue top-emitting organic light-emitting devices with highly saturated color” –*Current Applied Physics*, **4**, (2004) 663.
2. S. N. Lee, S. F. Hsu, S. W. Hwang and Chin H. Chen, “Effects of substrate treatment on the electroluminescence performance of flexible OLEDs” –*Current Applied Physics*, **4**, (2004) 651.
3. I. R. Laskar, S. F. Hsu and T.-M Chen, “Syntheses, photoluminescence and electroluminescence of some new blue-emitting phosphorescent iridium(III)-based materials” –*Polyhedron*, **24**, (2005) 189.
4. S. J. Yeh, W. C. Wu, C. T. Chen; Y. H. Song, Y. Chi; M. H. Ho, S. F. Hsu, Chin H. Chen “New dopant and host materials for blue phosphorescent organic electroluminescent devices” –*Advanced Materials*, **17**, (2005) 285.
5. S. F. Hsu, C. C. Lee, A. T. Hu, S. W. Hwang, H. H. Chen, and C. H. Chen, “Color-saturated and highly efficient top-emitting organic electroluminescent devices” –*Thin Solid Films*, **478**, (2005) 271.
6. I. R. Laskar, S. F. Hsu and T.-M Chen, “Highly Efficient Orange-Emitting OLEDs Based on Phosphorescent Platinum(II) Complexes” –*Polyhedron*, **24**, (2005) 881.
7. S. F. Hsu, C. C. Lee, S. W. Hwang, and C. H. Chen “Highly efficient top-emitting white organic electroluminescent devices” –*Applied Physics Letters*, **86**, (2005) 253508. (**highlighted by news report in *Photonics Spectra***).
8. I. R. Laskar, S. F. Hsu and T.-M Chen, “Investigating photoluminescence and electroluminescence of iridium(III)-based blue-emitting phosphors” –*Polyhedron*, **26**, (2006) 1167.
9. T. H. Liu; S. F. Hsu, M. H. Ho, C. H. Liao; Y. L. Tung, P. C. Wu, Y. Chi; Chin H. Chen, “Phosphorescence of red Os(fppz)₂(PPh₂Me)₂ doped organic light-emitting devices with *n*- and *p*-hosts” –*Applied Physics Letters*, **88** (2006) 063508.
10. S. F. Hsu, I. R. Laskar, T.-M. Chen, J.-W. Ma, S.-W. Hwang and Chin H. Chen, “Highly efficient yellowish-white phosphorescent organic light-emitting devices” –*Japanese Journal of Applied Physics*, **45** (2006) L951.

B. Conference papers

1. "Fabrication of transparent cathode for top-emitting organic light emitting devices" –S. F. Hsu, C. C. Lee and C. H. Chen, *Proceedings of The 4th International Conference on Electroluminescence of Molecular Materials and Related Phenomena (ICEL-4)*, Korea, 2003.
2. "Effects of substrate treatment on the EL performance of flexible OLEDs" –S. N. Lee, S. F. Hsu, S. W. Hwang, C. H. Chen, *Proceedings of The 4th International Conference on Electroluminescence of Molecular Materials and Related Phenomena (ICEL-4)*, Korea, 2003.
3. "Structural Effect of BAIs on the EL Performance of Phosphorescent Organic Electroluminescent Devices" by Y. S. Wu, S. F. Hsu, H. H. Chen and C. H. Chen, *Proceedings of The 10th International Display Workshop (IDW '03)*, p.1343, Fukuoka, Japan, 2003.
4. "Top-emitting organic light-emitting devices for full color displays" –S. F. Hsu, C. C. Lee, A. T. Hu and C. H. Chen, *Proceedings of The Taiwan Display Conference (TDC '04)*, p.340, Taipei, Taiwan, 2004.
5. "Novel host materials for phosphorescent organic light emitting devices" –M. H. Ho, Y. S. Wu, S. F. Hsu, T. Y. Chu, J. F. Chen, and C. H. Chen, *Proceedings of The 11th International Display Workshop (IDW '04)*, p. 1319, Niigata, Japan, 2004.
6. "White light top-emitting light-emitting devices" –S. F. Hsu, S. W. Hwang, and C. H. Chen, *Proceedings of The International Display Manufacturing Conference 2005 (IDMC '05)*, p. 691, Taipei, Taiwan, 2005.
7. "Three-wavelength white electrophosphorescence with two emissive materials" –S. F. Hsu, I. R. Laskar, T. M. Chen and Chin H. Chen, *Proceedings of The International Display Manufacturing Conference 2005 (IDMC '05)*, p. 694, Taipei, Taiwan, 2005.
8. "Highly efficient top-emitting white organic electroluminescent devices" –S. F. Hsu, S. W. Hwang, and C. H. Chen, *SID International Symposium 2005 (SID2005)*, p. 32, Boston, USA, 2005. **(Oral)**.
9. "Blue Dopants and New Host Materials for Phosphorescent Organic Light-Emitting Diodes" –C. T. Chen, S. J. Yeh, M. F. Wu, Y. Chi, Y. H. Song, M. H. Ho, S. F. Hsu, Chin. H. Chen, *SID International Symposium 2005 (SID 2005)*, p. 1756, Boston, USA, 2005. **(Oral)**.

10. “Controlling recombination zone in *p-i-n* white organic light-emitting diode” –J.-W. Ma, S.-W. Hwang, C.-C. Chang, S. F. Hsu, Chin H. Chen, *SID International Symposium 2006 (SID 2006)*, p. 964, San Francisco, USA, 2006.
11. “Highly efficient top-emitting organic light-emitting devices” –S. F. Hsu, S. W. Hwang, C. H. Chen, S.-H. Lee, and C.-C. Lee, *SID International Symposium 2006 (SID 2006)*, p. 1201, San Francisco, USA, 2006. **(Oral)**.
12. “White organic light-emitting diodes with *n*-type and *p*-type doped transporting layers” –P.-C. Yeah, J.-W. Ma, S.-W. Hwang, S. F. Hsu, C.-J. Chen, and C. H. Chen, *Proceedings of The 6th International Conference on Electroluminescence of Molecular Materials and Related Phenomena (ICEL-6)*, Hong Kong, 2006.

C. Chinese journals

1. 徐士峯、李世男、李孟庭和陳金鑫，
“可撓曲式有機發光二極體元件材料及製程技術的研發”，*光訊*, 98 (2002) 7.
2. 鄭榮安、徐士峯和陳金鑫，
“有機電激磷光材料在 OLED 顯示器上的應用與發展”，*光學工程*, 79 (2002) 12.
3. 徐士峯、李重君和陳金鑫，
“上發光有機發光二極體的發展與應用”，*光訊*, 108 (2004) 1.

D. Patents

1. 陳金鑫、徐士峯、黃孝文、李重君和李世昊—“高效率白光上發光有機電激發光元件”(中華民國、US pending)
2. 陳金鑫、徐士峯、黃孝文、李重君和李世昊—“高效率易製作之白色有機電激發光元件”(中華民國、US pending)
3. 陳金鑫、徐士峯、黃孝文、李世昊和李重君—“新型 OLED 之電洞注入系統”(中華民國、US pending)

Author's autobiography



Shih-Feng Hsu was born in Taiwan in 1980. He received the B.S. degree from Department of Applied Chemistry from National Chiao Tung University (NCTU), Hsinchu, Taiwan in 2002. He joined in OLED research group in 2000 and has engaged in the synthesis of iridium-based phosphorescent emitters. He is pursuing his Ph.D. degree currently at Department of Applied Chemistry in NCTU under the guidance of Prof. C. H. Chen.

His research interests are studies of optical outcoupling effect and device engineering of highly efficient top-emitting organic light-emitting devices.

